# HYDROLYSIS OF ORGANOPHOSPHOROUS ESTERS INDUCED BY NANOSTRUCTURED TITANIA-BASED REPLICAS OF DIATOM MICROSHELLS

**A Thesis**
**Presented to**
**The Academic Faculty**

**by**

**Seungjin Lee**

**In Partial Fulfillment**
**of the Requirements for the Degree**
**Masters of Science in the**
**School of Civil and Environmental Engineering**

**Georgia Institute of Technology**
**August, 2006**

# HYDROLYSIS OF ORGANOPHOSPHOROUS ESTERS INDUCED BY NANOSTRUCTURED TITANIA-BASED REPLICAS OF DIATOM MICROSHELLS

Approved by:

Dr. Ching-Hua Huang, Advisor
School of Civil and Environmental Engineering
*Georgia Institute of Technology*

Dr. Kenneth H. Sandhage
School of Materials Science and Engineering
*Georgia Institute of Technology*

Dr. Jaehong Kim
School of Civil and Environmental Engineering
*Georgia Institute of Technology*

Date Approved: May 19, 2006

# ACKNOWLEDGEMENTS

I would like to thank my advisor Dr. Ching-Hua Huang for her guidance and support and the thesis committee members, Dr Kenneth H. Sandhage and Dr. Jaehong Kim for their valuable advice. I also thank my fellow graduate students and researchers for their friendship and kind help: Dr. Guangxuan Zhu, Dr. Huichun Zhang, Amisha Shah, Wan-Ru Chen, Sang-Hyuck Park, Edward McCallum, Piti Piyachaturawat, Samuel Shian, Shawn M. Allan, Dr. Benjamin Church, and Dr. Ye Cai. I would like to acknowledge the assistance provided by Earl Babbitt, Andre Bé, and Therese Rehkopf.

Special thanks go to Ted and Rebecca Brewer, Tony and Sunyoung Park, Alexander and Jinyang Chun, and Dr. Donghyun Kwon, who are my friends and helped my family both materially and spiritually.

The greatest thanks go to my family. I owe what I am to my parents, my father Taekjong Lee, my mother Uisook Song. The love and support of my wife, Inhee Huh is just beyond expression. My daughter Rebecca Eunjae Lee and my son Daniel Eunkhang Lee have been the source of my energy to live.

I acknowledge the financial support from National Science Foundation.

# TABLE OF CONTENTS

# LIST OF TABLES

# LIST OF FIGURES

# LIST OF SYMBOLS AND ABBREVIATIONS

| | |
|---|---|
| $k$ | pseudo-first-order rate constant |
| BA | benzoic acid |
| BET | Brunauer, Emmett and Teller |
| BJH | Barrett-Joiner-Halenda |
| EDX | Energy dispersive X-ray |
| MAMB | methyl 4-(aminomethyl)benzoate |
| MB | methyl benzoate |
| MES | 2-(*N*-morpholino)ethanesulfonic acid |
| MOPS | 4-morpholinepropanesulfonic acid |
| MOX | methyl paraoxon |
| MS | methyl salicylate |
| MTH | methyl parathion |
| NAM | Nanostructured and Amorphous Materials |
| $pH_{IEP}$ | pH of isoelectric point |
| SA | salicylic acid |
| SEM | Scanning electron microscopy |
| TEM | transmission electron microscopy |
| XRD | X-ray diffraction |

# SUMMARY

**Chapter 1.** Three-dimensional microscale assemblies of fluorine-doped titania nanoparticles, synthesized via the shape-preserving reactive conversion of silica-based diatom microshells, induce the rapid hydrolysis of methyl paraoxon and methyl parathion (insecticides and nerve agent mimics) under near neutral pH conditions in the absence of light.

**Chapter 2.** In our earlier work, silica-based diatom frustules were successfully converted to 3-dimesional F-doped titania-based replicas via shape-preserving gas/solid displacement reactions, and experiments showed that the hydrolysis of organophosphorous ester pesticides, methyl paraoxon (MOX) and methyl parathion (MTH) was significantly faster in the presence of these 3-D titania nanostructures than in the presence of other commercial titania nanoparticles. The enhancement effect of titania frustules appeared to be strongly related to the amount of F-doping on these materials. In this work, a wider range of titania frustule replicas with various F-doping were prepared and characterized, and compared in the hydrolysis of MOX and MTH as well as three carboxylic acids (methyl salicylate, methyl benzoate and methyl 4-(aminomethyl)benzoate). A strong relationship between the amount of F-doping and the enhancement effect on the hydrolysis of organophosphorous esters was still observed. However, such enhancement effect did not occur in the hydrolysis of the carboxylic acids. It was discovered that fluorine-leaching from the titania frustules was significant and yielded high concentration of fluoride ions in the reaction solutions. Dissolved

fluoride ions alone could significantly catalyze the hydrolysis of organophosphorous esters but not that of carboxylic acids in the oxide-free systems. It is believed that fluoride ions act as nucleophilic catalysts to accelerate the hydrolysis of organophosphorous esters. Comparison in the hydrolysis product formation from the two potential hydrolysis pathways (i.e., the P-O bond and the C-O bond cleavages) in the studied systems also supports the direct involvement of dissolved fluoride ions in the observed catalytic effect.

# CHAPTER 1. RAPID, NON-PHOTOCATALYTIC DESTRUCTION OF ORGANOPHOSPHOROUS ESTERS INDUCED BY NANOSTRUCTURED TITANIA-BASED REPLICAS OF DIATOM MICROSHELLS

Three-dimensional microscale assemblies of fluorine-doped titania nanoparticles, synthesized via the shape-preserving reactive conversion of silica-based diatom microshells, induce the rapid hydrolysis of methyl paraoxon and methyl parathion (insecticides and nerve agent mimics) under near neutral pH conditions in the absence of light.

An appreciable body of research has demonstrated that nano-sized or nanostructured metal oxides can exhibit superior catalytic activity due to exceptionally high surface areas, modified surface structures, and other nanoscale phenomena.[1-4] Indeed, the photo-catalytic degradation of environmental pollutants by titanium dioxide ($TiO_2$) nanoparticles has been extensively examined for several decades.[5-11] Here we report, for the first time, the use of three-dimensional, porous titania-based nanoparticle assemblies that greatly enhance the rate of hydrolysis of the organophosphorous esters, methyl paraoxon (MOX) and methyl parathion (MTH), in the absence of light and at near neutral pH conditions. MOX and MTH are widely used insecticides in crop and fruit production and home gardening, and are structural mimics of nerve agents.[12]

Three-dimensional (3-D) assemblies of titania nanoparticles were synthesized through the shape-preserving reactive conversion of the silica-based microshells (frustules) of diatoms. Diatoms (*Bacillariophyceae*) are single-celled eukaryotic phytoplankton that populate a wide range of aquatic environments.[13-18] Diatoms form rigid cell walls (frustules) comprised of intricate, porous, 3-D networks of amorphous silica nanoparticles.[13-18] Frustule morphologies are species specific; that is, each of the tens of thousands of diatom species assembles a frustule with a particular 3-D shape and with specific patterns of fine nanoscale features (pores, channels, protuberances) that are faithfully replicated upon cellular reproduction.[13-18] As a result, sustained reproduction of a given diatom species can yield enormous numbers of daughter diatoms with frustules of identical shape (e.g., 40 sustained reproduction cycles can yield $2^{40}$, or more than 1 trillion, frustule replicas).[19-21] Recent work has demonstrated that such precise and scalable silica-based assemblies can be converted into titania-based replicas through the use of the following gas/solid reactions:

$$2TiF_4(g) + SiO_2(s) \rightarrow 2TiOF_2(s) + SiF_4(g) \qquad (1)$$

$$2TiOF_2(s) + (1\text{-}a)O_2(g) \rightarrow 2TiO_{2\text{-}a}F_b(s) + (2\text{-}b)F_2(g) \qquad (2)$$

where $TiO_{2-a}F_b(s)$ refers to the fluorine-doped anatase polymorph of titania.[22-24] Specifically, cylindrical silica-based frustules of *Aulacoseira* diatoms were allowed to react with $TiF_4(g)$ at 350°C for 2 h (reaction (1)). Energy-dispersive x-ray (EDX) and x-ray diffraction (XRD) analyses indicated that reaction under these conditions resulted in complete conversion of the $SiO_2$ frustules into $TiOF_2$ replicas.[22-24] A second heat treatment was then conducted at 350°C for 2 h in flowing oxygen to convert the $TiOF_2$-based frustules into F-doped anatase $TiO_2$ as per reaction (2). The resulting anatase products again retained the starting frustule shape and fine features (nanoscale pores,

channels). Transmission electron microscopy (TEM) of product cross-sections indicated that the converted frustules consisted of a nanoporous network of anatase crystals with sizes on the order of 50 nm.[22-24]

The open, nanocrystalline nature of such 3-D anatase frustule replicas led the present authors to consider their use to enhance the rate of hydrolysis of pesticide-like compounds. Three types of replicas (labeled FI, FII, and FIII in Table 1-1) were prepared from *Aulacoseira* diatom frustules. The frustules were first converted into $TiOF_2$ via reaction (1) as described earlier.[22-24] FI replicas were given no further heat treatments. The FII and FIII replicas were exposed to a second heat treatment in moist oxygen (generated by passing oxygen through a water bath at 45°C) to allow for conversion into anatase titania. For the FII replicas, this second heat treatment was conducted at 400°C for 2 h, whereas a 600°C/5 h heat treatment was used for the FIII replicas. Two commercially available $TiO_2$ nanoparticles were also examined for comparison: 20 nm anatase/rutile particles (~75% anatase, 25% rutile,[25] P25, Degussa, USA) and 10 nm anatase particles (99% anatase, Nanostructured and Amorphous Materials, Houston, USA) that are referred to herein as P25 and NAM nanoparticles, respectively.

Batch kinetic experiments were conducted in 25-60 mL amber borosilicate bottles that were protected from light. Dry $TiO_2$ particles, buffered reagent water (10 mM acetic acid, 2-(N-morpholino)ethanesulfonic acid [MES], 4-morpholinepropanesulfonic acid [MOPS], and their corresponding sodium salt for pH ranges of 4-5, 5.5-7, and 7-8, respectively), 10 mM NaCl, and a stir bar were added to each bottle. The reactors were maintained at 22°C with constant stirring. After 1-2 h, an appropriate amount of pesticide stock solution (MOX or MTH obtained at >98% purity from Chem Service, West Chester, PA, USA; in a methanol/water mixture) was added to initiate reaction.

Table 1-1. Characteristics of frustule replicas (FI-FIII) and commercial titania nanoparticles (P25 and NAM).

| Particles | Particle Size | Specific Surface Area ($A_s$, $m^2/g$) | Isoelectric Point |
|---|---|---|---|
| P25 | 20 nm[d] | 54.4 ± 2.7 | 5.2 |
| NAM | 10 nm[d] | 311.6 ± 15.2 | 6.0 |
| FI[a] | 12 μm (dia.) × 16 μm (length)[e] | 2.1 ± 0.1 | 2.5 |
| FII[b] | | 4.2 ± 0.1 | 3.3 |
| FIII[c] | | 2.6 ± 0.2 | 4.3 |

[a]$TiOF_2$-based frustule replica; [b]$TiO_2$ frustule replica (5.5 wt% F); [c]$TiO_2$-based replica (1.4 wt% F); [d]from manufacturer, [e]from SEM images

The starting pesticide concentration was 100 μM and the initial titania loading was 1.0 g/L. The initial reaction solution contained 2.5 vol% methanol. Sample aliquots were periodically collected and centrifuged prior to analysis. The MOX, MTH, and their hydrolysis product, 4-nitrophenol (4-NP), were analyzed by an Agilent high performance liquid chromatography (HPLC) system with a Zorbax RX-C18 column (4.6 × 250 mm, 5μm) and a diode-array UV/Vis detector operating at 275 nm. The mobile phase consisted of solution of 1 mM phosphoric acid or trifluoroacetic acid and pure acetonitrile at 65:35 and 40:60 (v/v) ratios for methyl paraoxon and methyl parathion, respectively. A 5 min isocratic elution of 95:5 (v/v) acid solution:acetonitrile was applied prior to the above conditions.

The rates of hydrolysis of MOX and MTH in the presence or absence of titania were found to follow pseudo-first-order kinetics. Least-square linear regression analyses of plots of the log parent compound concentration versus time yielded lines with $R^2$ values greater than 0.96. The pseudo-first-order rate constants (obtained from the slopes of these lines) are shown in Table 1-2. In all of the experiments, the loss of MOX and MTH coincided with the generation of 4-NP, reaching >95% of overall mass balance throughout the reaction (an example is shown in Fig. 1-1).

As shown in Table 1-2, the hydrolysis rates of MOX and MTH were enhanced in the presence of all types of particles examined. However, the frustule replicas (particularly the FII specimens) were substantially more effective at increasing the hydrolysis rates than were the P25 and NAM nanoparticles. The relative rates of hydrolysis ($k/k_0$ values) of MOX over the pH range of 4.5-7.9 increased by factors of 102-129 in the presence of the FII replicas, whereas the P25 and NAM nanoparticles enhanced the rates by factors of 3.8-5.8 and 10.7-15.2, respectively. A similar, although

Table 1-2. Pseudo-first-order rate constants ($k$) for the hydrolysis of methyl paraoxon (MOX) and methyl parathion (MTH) in the presence and absence of commercial titania particles or frustule replicas.

| | | MOX | | MTH | |
|---|---|---|---|---|---|
| pH | $TiO_2$ particles | $k$ ($\times 10^{-4}$ $h^{-1}$) | $k/k_0$ [a] | $k$ ($\times 10^{-4}$ $h^{-1}$) | $k/k_0$ [a] |
| 4.5 | No oxide | 3.27 ± 0.53 | 1.0 | 1.57 ± 0.43 | 1.0 |
| | P-25 | 13.43 ± 1.52 | 4.1 | 7.59 ± 2.67 | 4.8 |
| | NAM | 42.50 ± 1.48 | 13.0 | 7.88 ± 1.61 | 5.0 |
| | FI | 222.9 ± 20.8 | 68.2 | 31.98 ± 1.37 | 20.4 |
| | FII | 334.9 ± 42.1 | 102.4 | 34.42 ± 3.60 | 21.9 |
| | FIII | 36.2 ± 1.36 | 11.07 | 6.21 ± 0.61 | 4.0 |
| 6.3 | No oxide | 3.62 ± 1.04 | 1.0 | 2.19 ± 0.50 | 1.0 |
| | P-25 | 20.90 ± 1.10 | 5.8 | 7.23 ± 1.83 | 3.3 |
| | NAM | 54.86 ± 4.50 | 15.2 | 12.38 ± 1.49 | 5.7 |
| | FI | 373.0 ± 35.1 | 103.0 | 38.07 ± 1.62 | 17.4 |
| | FII | 468.5 ± 101 | 129.4 | 40.31 ± 4.20 | 18.4 |
| | FIII | 68.54 ± 3.37 | 18.93 | 10.31 ± 1.19 | 4.7 |
| 7.9 | No oxide | 6.78 ± 0.72 | 1.0 | 2.98 ± 0.56 | 1.0 |
| | P-25 | 25.90 ± 1.25 | 3.8 | 12.60 ± 1.72 | 4.2 |
| | NAM | 72.32 ± 3.57 | 10.7 | 13.66 ± 3.22 | 4.6 |
| | FI | 507.9 ± 49.5 | 74.9 | 47.91 ± 2.65 | 16.1 |
| | FII | 799.3 ± 314 | 117.9 | 54.00 ± 6.56 | 18.1 |
| | FIII | 87.25 ± 4.86 | 12.9 | 11.56± 1.42 | 3.9 |

[a] $k_0$: the rate constant in the absence of $TiO_2$

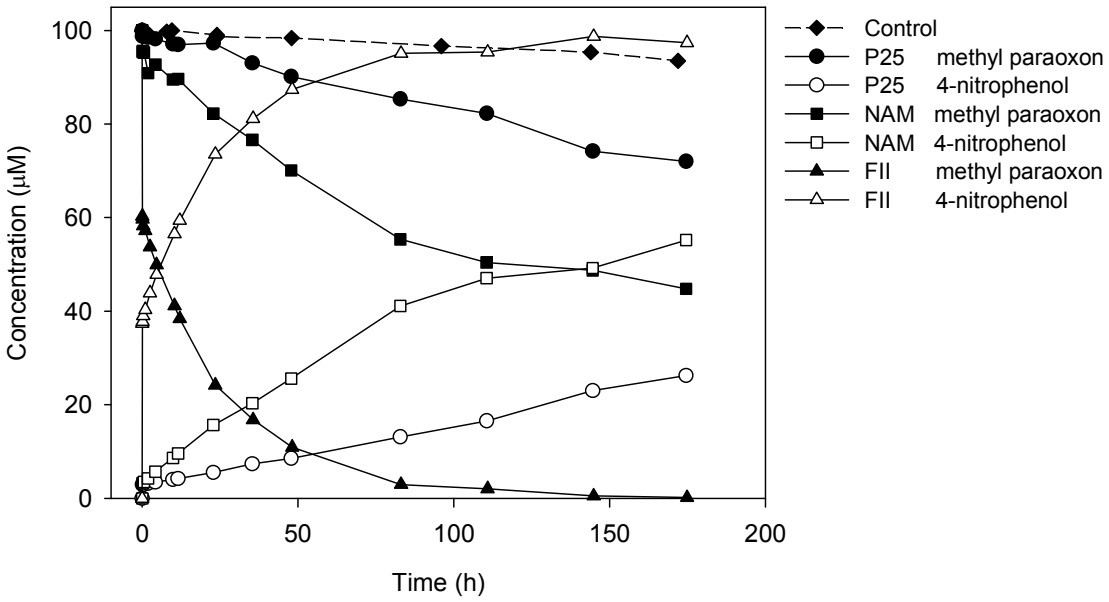


Figure 1-1(a). Reaction time course of methyl paraoxon (MOX) hydrolysis and 4-nitrophenol product generation in the presence and absence (control) of titania nanoparticles and titania-based frustule replicas.

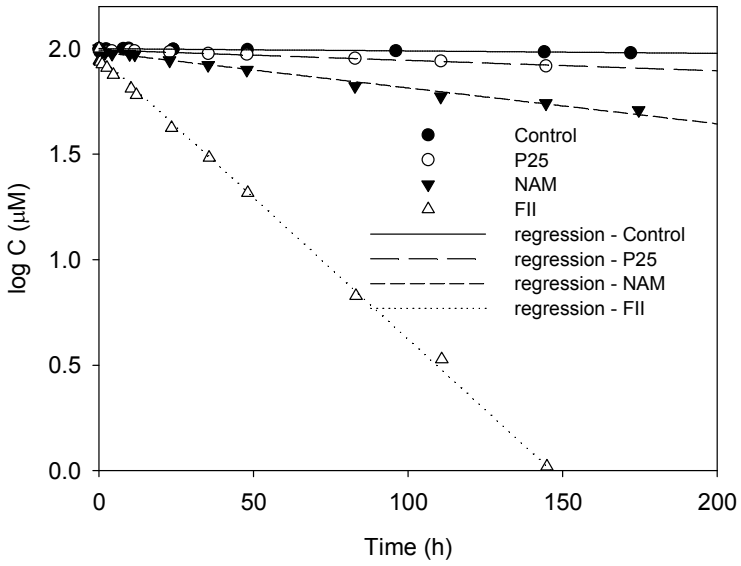


Figure 1-1(b). Plot of the log of MOX concentration versus time. Reaction conditions: 1.0g/L $TiO_2$, 100 μM methyl paraoxon initially, 10 mM NaCl, 5 mM acetate buffer (pH 4.5), 25°C.

less pronounced, trend was observed for the hydrolysis of MTH. The enhancements in the hydrolysis rates resulting from the titania frustule replicas decreased as the temperature used for conversion into anatase increased from 400°C to 600°C.

To obtain further insights into these observations, additional structural and chemical analyses were conducted on the particles and frustule replicas. The specific surface areas, $A_s$, were evaluated with $N_2$-adsorption (BET) analyses (ASAP 2000 Physi/Chemisorption unit, Micromeritics Instrument Corp., USA). Values of the isoelectric point were determined by measuring the zeta potentials (ZetaPlus analyzer, Brookhaven Instruments Corp., USA) of aqueous titania suspensions (0.1 g/L) as a function of pH (as shown in Fig. 1-2). The residual fluorine content of the anatase titania frustules was evaluated with a pyrohydrolysis method (see Fig. 1-3).[26] An alumina crucible containing 100 mg of the titania frustules was placed inside a controlled atmosphere tube furnace. The furnace was heated at 10°C/min to 950°C and held for one hour at this temperature. At this temperature, a flowing $H_2O/O_2$ gas mixture was introduced into the furnace by passing pure oxygen (1 liter/minute) through a water bath heated to 45°C. The hydrofluoric acid vapor generated by the reaction of the water vapor with fluorine from the titania frustules was trapped in an acetate buffered solution (a 1 L aqueous solution containing 10 g potassium acetate and 5 mL acetic acid, pH = 4.3) located downstream of the frustules. The fluorine content of the trap solution was evaluated with a fluoride ion-selective electrode that was calibrated against standard fluoride solutions (Denver Instrument, USA).

Although more effective at enhancing the hydrolysis rates of MOX and MTH, the titania frustule replicas possessed substantially lower specific surfaces areas (2.6-4.2 m2/g) than the P25 (54.4 $m^2/g$) and NAM (311.6 $m^2/g$) nanoparticles. In other words, the

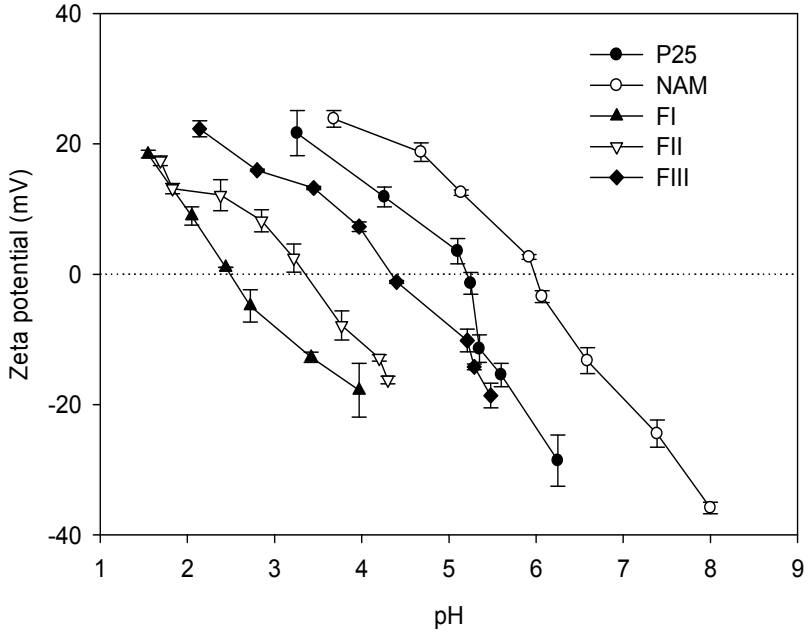


Figure 1-2. Zeta potentials of titania nanoparticles and titania-based frustule replicas in aqueous suspensions ([$TiO_2$] = 0.1 g/L) as a function of pH

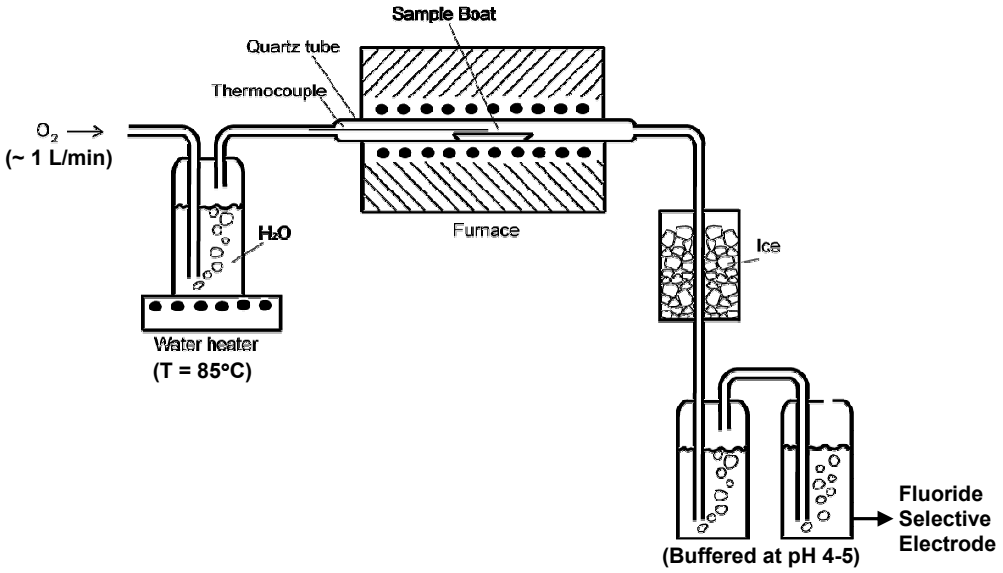


Figure 1-3. Schematic of the pyrohydrolysis setup to measure the fluorine content in the titania-based frustule replicas.

influence of the anatase frustule replicas on hydrolysis became even more pronounced when the particle surface areas were taken into account. For example, the values of the specific relative rate constants ($k/[k_0A_s]$) for MOX hydrolysis in the presence of the FII particles were 290-400 and 590-820 times higher than in the presence of the P25 and NAM nanoparticles, respectively!

No appreciable differences were detected in the morphologies (from SEM analyses, Fig. 1-4) or specific surface areas of specimens FI, FII, and FIII (Table 1-1). However, these frustule replicas possessed significant differences in fluorine contents and isoelectric points. Upon conversion of TiOF2 into anatase at 400$^o$C, the fluorine content dropped to 5.5 wt% (note: the compound TiOF2 contains 37.3 wt% fluorine). After conversion at 600$^o$C, the fluorine content decreased to 1.4 wt%. The decline in residual F-content coincided with a decrease in the surface acidity (i.e., increasing $pH_{IEP}$) of the frustule replicas. The isoelectric points of specimens FII and FIII ($pH_{IEP}$ = 3.3 and 4.3, respectively) were also considerably lower than is typically reported for anatase-based powders (e.g., the isoelectric points measured for the P25 and NAM powders were 5.2 and 6.0, respectively).[27,28]

It is well known that metal ions can catalyze the hydrolysis of carboxylic esters, amides, and phosphorous esters by (i) coordinating such compounds in a manner that raises their susceptibility towards nucleophilic attack, (ii) coordinating the nucleophile in a manner that raises its reactivity toward electrophilic sites, or (iii) a combination of these mechanisms.[29-31] Mechanism (i) is strongly related to the ability of metal ions to coordinate the compound (e.g., the O atom of the P=O bond) and polarize electrons away from the nucleophilic site (e.g., the P center of the P=O bond). Mechanism (ii) is

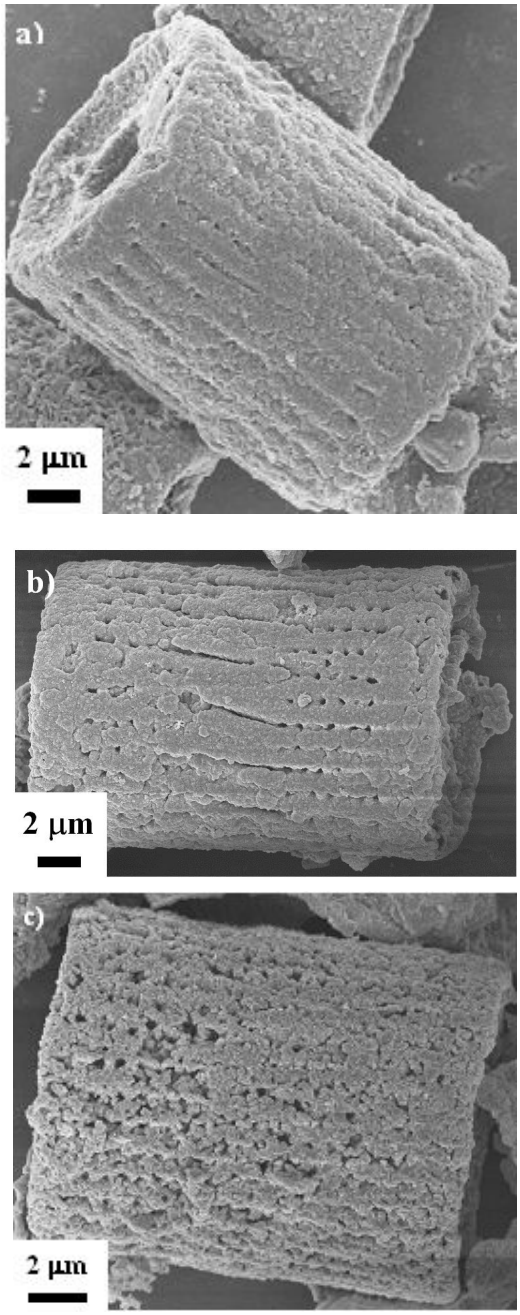


Figure 1-4. Scanning electron images of the frustule replicas: a) FI ($TiOF_2$-based), b) FII ($TiO_2$-based, with 5.5 wt% F) and c) FIII ($TiO_2$-based, with 1.4 wt% F).

strongly tied to the ability of metal ions to induce the deprotonation of coordinated water through reactions such as: $Me^{2+} + H_2O = MeOH^+ + H^+$ , $*K_1 = [MeOH^+][H^+]/[Me^{2+}]$. Thus, metal ions of stronger Lewis acidity and greater affinity to the compound ligand donor atoms would be stronger catalysts. The catalysis of metal oxide surfaces on hydrolysis reactions is essentially similar to that of dissolved metal ions.[28,32-35] In addition, other factors such as surface area, charge, morphology and active site density may also play a role.

Based on the above discussion, the stronger surface acidity of the titania frustule replicas due to F-doping likely led to the enhanced hydrolysis of MOX and MTH relative to the P25 and NAM titania particles. Earlier studies have documented that fluorine incorporation in alumina and silica-alumina catalysts (with F replacing surface or lattice O and OH groups) increased the acidity of both protonic (Bronsted) and nonprotonic (Lewis) sites on the surfaces, owing to the stronger electronegativity and polarizing effect of fluorine.[36,37] F-modified alumina has exhibited enhanced catalytic activity for reactions such as cracking, isomerization, alkylation, disproportionation, and polymerization.[36,37] By analogy, the presence of fluorine in the anatase titania of this study likely resulted in increased Lewis acidity and excess positive charge on the surface-bound Ti(+IV), as indicated by the lower $pH_{IEP}$ values of the titania frustule replicas. The enhanced susceptibility of MOX to hydrolysis, relative to MTH, in the presence of the titania frustule replicas can also be explained. MOX possesses a "hard" O donor that is likely to coordinate more strongly to the "hard" Ti(+IV) metal center than MTH's "soft" S donor,[38] thus rendering a greater susceptibility for hydrolysis via the mechanism (i) discussed above. Sulfur is also less electro-negative than oxygen, resulting in a less

electrophilic (and thus less reactive) phosphorous center in the thionates than in the oxonates.

This work provides the first report of the enhanced hydrolysis of pesticide-like compounds resulting from the presence of porous 3-D assemblies of nanocrystalline F-doped anatase $TiO_2$ under near neutral conditions and in the absence of light (non-photocatalytic conditions). The enhanced activity of such nanostructured titania assemblies without the need for a strong UV light source is quite attractive for the hydrolytic destruction of environmental pollutants in remote locations. Furthermore, $SiO_2$-based diatomaceous earth, which has long been used in water purification applications,[39] is readily available in large quantities at low cost, and the chemical conversion technique employed in this study is a scalable means of converting diatomaceous earth into fluorine-doped titania nanoparticle structures. Although not a focus in this study, fluorine doping has been found to improve the photocatalytic activity of anatase towards the decomposition of acetaldehyde, trichloro-ethylene, acetone, and phenol.[40-42] Further research aimed at probing the photocatalytic effects of these nanostructured assemblies on pesticide hydrolysis and other types of reactions could be quite fruitful and is currently under way.

This material is based upon work partially supported by the National Science Foundation (Dr. Patrick Brezonik, Program Manager) and Air Force Office of Scientific Research (Dr. Joan Fuller, Dr. Hugh DeLong, Program Managers).

# CHAPTER 2. HYDROLYSIS OF ORGANOPHOSPHOROUS ESTERS INDUCED BY NANOSTRUCTURED TITANIA-BASED REPLICAS OF DIATOM MICROSHELLS: SIGNIFICANT EFFECT OF FLUORIDE IONS

## 2.1. Introduction

Inorganic metal oxides, aside from their numerous industrial applications, are very well known catalysts for pollutant degradation in the environment by various mechanisms such as hydrolysis, photolysis, and redox reactions.[43] A fast growing number of studies have demonstrated that nano-sized or nanostructured metal oxides can exert superior catalytic activity due to exceptionally high surface areas, modified surface properties, and other nanoscale phenomena.[1-4] For instance, superfine $Fe_2O_3$ nanoparticles were shown to be much more effective catalysts for the removal of carbon monoxide by oxidation or disproportionation than the non-nano oxide powder,[2] and the nanoparticles of ZnO, CuO/ZnO and NiO were more active than the commercially available materials with larger size to catalyze $CO_2$ conversion to $CH_3OH$.[1]

Owing to their excellent semiconductor properties, stability with respect to corrosion, and biological and chemical inertness, titanium dioxide ($TiO_2$) nanoparticles have been intensively investigated for photolytic degradation of various environmental pollutants for several decades. Nanosized $TiO_2$ particles have been proved by several studies to exhibit higher reactivity compared to the larger particles of such oxides.[5-11] These prior studies have often attributed the enhanced catalytic effect to the properties

such as high surface area, small particle size,[3] and crystallinity or defects of $TiO_2$ nanoparticles.[4]

In addition to the trend in developing nanosized and nanostructured features, significant amount of efforts have been made to modify the surface of metal oxide catalysts to achieve even better catalytic activity. Different modification processes have been adopted. Examples include doping foreign atoms such as S[44] and N[45] onto $TiO_2$ to expand the absorption spectra of $TiO_2$ into the visible light range, and doping carbon to change the surface character from hydrophilic to hydrophobic.[46] The carbon-black-modified nano-$TiO_2$ showed excellent catalytic efficiency in degrading refractory organic pollutants in photocatalytic ozonation.[47] In other studies, metals such as Pt,[48] Ag, V, Mn, and Fe[49] have been incorporated into $TiO_2$ to enhance the catalytic activity of $TiO_2$ but with limited success. Other modifications examined previously include coating of porous silica on the $TiO_2$ resulting in the rate enhancement of photocatalytic degradation of quaternary amines,[50] and soft mechanical activation of $TiO_2$ particles by low-energy mechanical milling inducing the alteration of intrinsic physicochemical properties and a decrease in the photocatalytic activities for the photocatalytic Cr(VI) reduction.[51]

Among the above efforts, several studies report on the modification of metal oxides with fluorine. For example, Adamczyk *et al*. reported that fluorine-modified chromium oxide (i.e., chromium oxofluorides) exhibited a significantly higher catalytic activity in the halogen exchange reactions (i.e., dismutation of $CCl_2F_2$ and fluorination of $CH_2ClCF_3$ with HF) than pure $CrF_3$ or $Cr_2O_3$.[52] Seo *et al*. reported that fluorine doping of alumina enhanced its catalytic effect on the conversion of *n*-butene to various hydrocarbons via oligomerization and cracking, and to isobutene via skeletal isomerization; the distribution between these two competing processes was strongly

affected by the amount of fluorine doping on the alumina.[36] In general, these studies mostly attributed the increased catalytic activity to the incorporation of F in the oxide lattice and the resulted increased Lewis sites due to the strong electronegativity of fluorine.[36,37,52]

In addition, fluorine doping of $TiO_2$ was reported to yield increased photocatalytic activity. The study by Yu *et al*. demonstrated that F-doped $TiO_2$ exhibited a stronger photocatalytic activity in the gaseous phase oxidation of acetone than the Degussa P25 $TiO_2$ which is a widely recognized excellent photocatalyst.[42] The authors reported that the F-doped $TiO_2$ samples exhibited stronger adsorption in the UV-visible range with a red shift in the band gap transition. The study by Li *et al*. demonstrated enhanced photocatalytic decomposition of acetaldehyde and trichloroethylene by F-doped $TiO_2$ under visible light range.[40] In contrast, their study indicates that F-doping had less effect on the optical absorption property of bulk $TiO_2$, while created oxygen vacancies on the surfaces that could be excited by lower energy and thus enhanced photocatalytic activity. In addition, studies also showed that complexation of $TiO_2$ surface with fluoride ions increased the photocatalytic activity compared to pure $TiO_2$ in the degradation of phenol.[41,53]

Aside from its wide use in photocatalytic applications, $TiO_2$ particles (as well as other metal oxides such as alumina) may also exhibit catalytic effect toward hydrolysis of organic compounds.[28,33,35] The catalysis of metal oxide surfaces on hydrolysis reactions is in principle similar to that of dissolved metal ions which can coordinate and polarize organic compounds at suitable functional groups via their Lewis acidity properties. Only a limited number of studies have investigated surface-catalyzed hydrolysis. However, the relevance of metal-catalyzed hydrolysis is widely demonstrated in biological systems as

many metabolic enzymes consist of metal ion centers to catalyze hydrolysis reactions and such catalysis has long been an interest to inorganic biochemists.[54] The potential catalytic effect of novel $TiO_2$ nanomaterials on hydrolysis reactions is the main focus in this study.

Although methods for massproducing titania-based materials with simple shapes are well established, appreciable global effort is being expended to develop scalable approaches for fabricating titania-based microassemblies with intricate, 3-D morphologies and precisely controlled fine (< 103 nm) features. Diatoms (*Bacillariophyceae*) are single-celled eukaryotic phytoplanktons that populate a wide range of aquatic environments.[13-18] Diatoms form rigid cell walls (frustules) comprised of intricate, porous, 3-D networks of amorphous silica nanoparticles.[13-18] Frustule morphologies are species specific; that is, each of the tens of thousands of diatom species assembles a frustule with a particular 3-D shape and with specific patterns of fine nanoscale features (pores, channels, protuberances) that are faithfully replicated upon cellular reproduction.[13-18] As a result, sustained reproduction of a given diatom species can yield enormous numbers of daughter diatoms with frustules of identical shape (e.g., 40 sustained reproduction cycles can yield $2^{40}$, or more than 1 trillion, frustule replicas).[19-21] Our recent work has demonstrated that such precise and scalable silica-based assemblies can be converted into titania-based replicas through the use of the gas/solid reactions.[22] As will be discussed further later, the silica-based diatom assemblies can be converted into titania-based frustule replicas through the use of gas/solid reactions (1) and (2):

$$2TiF_4(g) + SiO_2(s) \rightarrow 2TiOF_2(s) + SiF_4(g) \qquad (1)$$

$$2TiOF_2(s) + (1\text{-}a)O_2(g) \rightarrow 2TiO_{2\text{-}a}F_b(s) + (2\text{-}b)F_2(g) \qquad (2)$$

where $TiO_{2-a}F_b(s)$ refers to F-doped titania.[22-24] The resulting anatase products retained the starting frustule shape and fine features (nanoscale pores, channels). We also discovered that these biologically-derived 3-D titania nanostructures catalyze the hydrolysis of organophosphorous pesticides, methyl paraoxon (MOX) and methyl parathion (MTH) much more effectively than commercially available titania nanoparticles including Degussa P25 that have significantly larger surface areas.[55] The catalytic effect appeared to be strongly related to the amount of F-doping in these 3-D titania replicas.[55]

The objective of this current investigation is to further elucidate the mechanisms involved in the enhanced catalytic effect of 3-D titania diatom replica on the hydrolysis of MOX and MTH. In addition, another class of hydrolyzable compounds, i.e., carboxylic esters, are also included in this study. As will be shown later, $F^-$ ions leaching from 3-D titania replicas was discovered and thus the effect of $F^-$ ions alone on the hydrolysis was also examined. Generation of hydrolysis products in different reaction systems was characterized and compared to facilitate result interpretation.

## 2.2. Materials and Methods

### 2.2.1. Chemicals

Analytical standards of MOX and MTH, were obtained from Chem Service at >98% purity (Chem Service, West Chester, PA, USA) and used without further purification. Stock solutions of these two compounds were prepared by dissolving them in HPLC grade methanol and stored at -10$^{o}$C in the freezer. Other chemicals employed in this study including 4-nitrophenol (4-NP), salicylic acid (SA), benzoic acid (BA), methyl salicylate (MS), methyl benzoate (MB), methyl 4-(aminomethyl)benzoate (MAMB) hydrochloride, phosphoric acid, acetic acid, 2-(*N*-morpholino)ethanesulfonic acid (MES), 4-morpholinepropanesulfonic acid (MOPS), sodium borate, and sodium fluoride, were obtained from Aldrich (St. Louis, MO, USA) or Fisher Scientific (Fairlawn, NJ, USA) at a greater than 97% or of HPLC grade, and were used without further purification. All stock solutions (e.g., buffers, stock solutions) of these compounds were prepared using Milli-Q purified water (Millipore, MA, USA).

### 2.2.2. Preparation and Characterization of $TiO_2$ Materials

Titania-based replicas were prepared by converting the silica-based diatom assemblies through the use of the gas/solid reactions. Specifically, silica-based frustules of *Aulacoseira* diatoms were allowed to react with $TiF_4$(g) at 350°C for 2 h and were first converted into $TiOF_2$ as described earlier.[22-24] Six types of replicas (I-VI) were prepared from *Aulacoseira* diatom frustules according to the previously described procedure with

variation only in the annealing temperature. FI replicas were given no further heat treatments (i.e., the reaction (2)). FII through FVI replicas were exposed to a second heat treatment (i.e., the reaction (2)) in moist oxygen (generated by passing oxygen through a water bath at 45$^{o}$C) to allow for conversion into anatase titania. For the FII replicas, this second heat treatment was conducted at 400$^{o}$C for 2 hours, whereas a 600$^{o}$C/5 h heat treatment was used for the FIII - FVI replicas.

Two commercially available $TiO_2$ nanoparticles were also examined for comparison. The 20 nm anatase/rutile particles consisting of ~75% anatase and ~25% rutile,[25] (i.e., P25) were obtained from Degussa (USA). The 10 nm anatase particles (99% anatase) were obtained from Nanostructured and Amorphous Materials (Houston, TX, USA) and are referred to as NAM. The P25 nanoparticles, in particular, are among those most widely used in catalysis studies.

The BET surface area, BJH pore volume, and average pore volume of the oxides were determined based on an $N_2$ adsorption method using the ASAP 2000 (Micromeritics, Norcross, USA). A scanning electron microscope (SEM) (LEO 1530, Germany) with energy dispersive X-ray spectroscopy (EDX) capability was used for imaging, sizing and localized elemental analysis. High resolution imaging and selected area diffraction analysis using a transmission electron microscope (TEM) (Model 4000EX, JEOL, Japan) was conducted on the converted titania frustule replicas to get the morphology and phases.

Zeta potentials of various titania suspensions were measured by a zeta potentiometer (ZetaPlus, Brookhaven Instrument, NY, USA). The concentration of titania in the aqueous suspension was 0.1 g/L and the pH of the solution was varied by

adding small amount of strong acid or base. The pH of isoelectric point (i.e., the point of zero zeta potential; $pH_{IEP}$) of titania was obtained from the zeta potential versus pH plots.

The amount of residual fluorine in the titania frustules was determined by using a pyrohydrolysis setup[26] as shown in Fig. 1-3. An alumina crucible with about 100 mg of the powder sample was placed inside a furnace. The furnace was heated to 950°C at a 10°C/min heating rate and held for one hour while a stream of moisted oxygen gas (1 liter per minute, water heater temperature: 85°C) was passed through the sample tube. During this treatment, fluorine reacted with water and formed hydrofluoric acid gas. Water pre-mixed with buffer solution (a mix of 10 g potassium acetate and 5 mL acetic acid and diluted with water to 1 L) was utilized at the end of vapor stream to trap the acid gas. A fluoride ion-selective electrode (Denver Instrument, USA) was used to determine the fluoride potential in the trap solution and the overall fluorine content in the frustule sample was calculated by comparing the potential to a prepared standard curve.

### 2.2.3. Kinetic experimental setup

All glassware was soaked in 5 N $HNO_3$ for more than two days, rinsed with Milli-Q pure water, and dried in an oven maintained at 105°C prior to use. Batch hydrolysis kinetic experiments were conducted in 25-60 mL screw-cap amber borosilicate bottles with Teflon septa that were protected from light. Dry $TiO_2$ particles, buffered reagent water (5 mM of acetic acid for pH 4-5, 2-(N-morpholino)ethanesulfonic acid (MES) for pH 5.5-7, and 4-morpholinepropanesulfonic acid (MOPS) for pH 7-8, and borate for pH 9-10), 10 mM NaCl, and a stir bar were added to each bottle. The reactors were maintained at 22°C with constant stirring using a multi-position stir plate. After 1-2

h, an appropriate amount of a parent ester compound was added to initiate the reaction. The final reaction solution of MOX and MTH contained 2.5% (v/v) of methanol. Reactions typically contained 100 μM of the parent ester initially and 1.0 g/L of $TiO_2$ particles. Sample aliquots were periodically collected and centrifuged at 12,000 rpm for 20 min prior to analysis.

Adsorption of SA and BA were performed in borosilicate amber vials with continuous shaking on a shaker at 230 rpm. The solution pH was maintained at pH 4 (5 mM acetic acid) and 7 (5mM MOPS) for SA and 3 (5 mM phosphoric acid) and 7 (5 mM MOPS) for BA. After three days, sample aliquots were taken and centrifuged for 20 min before analysis.

The leaching of fluoride ions from the frustules was monitored as a function of time. Titania frustules were first added into a buffered solution at pH 7 to give 1.0 g/L aqueous suspension and the final pH was adjusted to pH 7 by adding a small amount of strong base. The potential of the solution was periodically monitored and the concentration of fluoride ions was calculated using a calibration curve established by sodium fluoride standards.

### 2.2.4. Analytical monitoring

Concentrations of the parent compounds and some of their hydrolysis products were monitored using an Agilent 1100 reverse-phase high performance liquid chromatography (HPLC) with a Zorbax RX-C18 column (4.6 × 250 mm, 5μm) and a diode-array UV/vis detector. MOX, MTH and 4-NP were monitored at 275 nm. MS and SA were monitored at 237 nm while MB, MAMB and BA at 230 nm. The mobile phase

consisted of 1 mM phosphoric acid or trifluoroacetic acid or pure acetonitrile at 65:35 (v/v) ratio for MOX and 40:60 (v/v) ratio for the other compounds. A 5 min isocratic elution of 95:5 (v/v) acid solution:acetonitrile was applied prior to the above conditions. SA, MA, MS, MB, and MAMB were also analyzed using the same method parameters mentioned above except the detection wavelengths used for salicylate and benzoate at 237 nm and 230 nm, respectively.

Hydrolysis products were identified by a HPLC system with a mass spectrometer (LC/MS) (1100MSD, Agilent Technology, USA). Sample aliquots taken periodically from reaction solutions were centrifuged for 20 min and the supernatants were analyzed by LC/MS. The MS analysis was conducted by electrospray ionization either in positive or negative mode at 80-175 fragmentation voltage with a mass scan range of 100-1000 m/z. The drying gas was operated at 10 mL/min at 350$^{o}$C. The nebulizer pressure was 25 psi, and the capillary was set at 4000 V.

## 2.3. Results and discussion

### 2.3.1. Properties of titania frustules

As discussed earlier, the silica-based diatom assemblies were converted into titania-based frustule replicas through the use of gas/solid reactions (1) and (2). After the reaction (1) (conditions described in 2.2), the silica-based assemblies were converted to $TiOF_2$. Energy dispersive x-ray (EDX) and X-ray diffraction (XRD) analyses indicated that this reaction resulted in complete conversion of the $SiO_2$ frustules into $TiOF_2$ replicas (FI). The reaction (2) was a "de-fluorination" heat treatment (conducted at 400°C for 2 hours for FII and 450-600°C for 5 hours for FII-VI in flowing oxygen) to convert the $TiOF_2$-based frustules into F-doped anatase $TiO_2$. The anatase crystalline structures of these F-doped $TiO_2$ frustules were confirmed by XRD analyses.[22] The SEM images of the resulting anatase replicas are shown in Fig. 2-1. As demonstrated by Fig. 2-1, this conversion technique preserved the original frustule shape and fine features (nanoscale pores, channels in the frustule wall). Also, there were no appreciable differences in the morphologies among the different titania frustule specimens that were prepared at different temperature for the reaction (2) (Fig. 2-1). Transmission electron microscopy (TEM) of cross-sections of the converted frustules indicated that the converted frustules consisted of a porous network of $TiO_2$ crystals with sizes on the order of 50 nm.[22-24]

Table 2-1 summarizes a range of properties of the $TiO_2$ frustule replicas and commercially obtained $TiO_2$ particles that were characterized in this study. Compared to the anatase frustules, the commercial titania particles P25 consist of approximately 75% of anatase and 25% of rutile[25] whereas the NAM particles consist of nearly 99% of

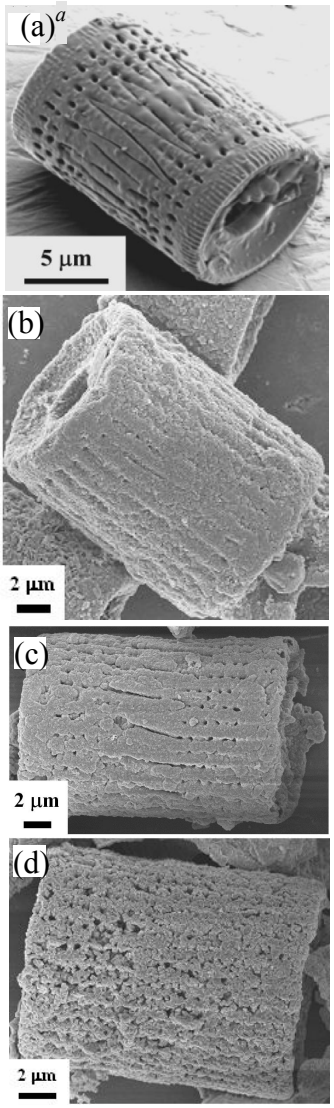


Figure 2-1. Scanning electron images of *Aulacoseira* diatom and the frustule replicas: (a) before treatment, (b) FI ($TiOF_2$-based), (c) FII ($TiO_2$-based, with 5.5 wt% F) and (d) FIII ($TiO_2$-based, with 1.4 wt% F). [a] from reference 22.

Table 2-1. Characteristics of titania frustules and nanoparticles.

| Metal Oxide | Crystalline Structure | Second Anneal Temp. | Particle Size | BET Surface Area ($m^2/g$) | BJH Pore Vol. ($cm^3/g$) | Ave. Pore Dia. (Å) | pH of Isoelec. Point | F-content % by wt |
|---|---|---|---|---|---|---|---|---|
| P25 | 75% anatase 25% rutile [a] | - | 21 nm [a] | 54.37 ± 2.70 | 0.132 | 114 | 5.2 | - |
| NAM | anatase [a] | | 10 nm [a] | 311.6 ± 15.2 | 0.324 | 77 | 6.0 | - |
| FI | $TiOF_2$ [b] | w/o oxidation | | 2.06 ± 0.05 | 0.076 | 222 | 2.5 | 27.3 ± 4.5 |
| FII | | 400 °C | | 4.17 ± 0.07 | 0.011 | 474 | 3.3 | 5.5 ± 0.2 |
| FIII | | 450 °C | 10 μm(φ) × | 3.54 ± 0.05 | 0.010 | 126 | 4.0 | 4.9 ± 0.6 |
| FIV | anatase [b] | 480 °C | 20 μm(h) [c] | 4.17 ± 0.12 | 0.012 | 125 | 4.1 | 4.5 ± 0.9 |
| FV | | 500 °C | | n.a. | n.a. | n.a. | - | 4.4 ± 0.2 |
| FVII | | 600 °C | | 2.59 ± 0.16 | 0.009 | 102 | 4.3 | 1.4 ± 0.2 |

[a] from manufacturers; [b] determined by XRD; [c] based on SEM images; n.a. = not available

anatase phase according to the manufacturer. $TiO_2$ frustules have a diameter of approximately 10 μm and a height of about 20 μm based on SEM images (Fig. 2-1). In contrast, P25 and NAM have much smaller reported particle diameters (21 nm and 10 nm, respectively) by the manufacturers. The BET analysis indicates that the $TiO_2$ frustules have much lower specific surface areas (2.1 - 4.2 $m^2/g$) than P25 and NAM titania particles (i.e., 54.5 $m^2/g$ and 311.6 $m^2/g$, respectively). The $TiO_2$ frustules also appeared to have smaller pore volumes than the commercial titania particles (Table 2-1).

According to the $pH_{IEP}$ values obtained from the zeta potential measurement (Fig. 2-2), titania frustules exhibit considerably lower isoelectric points ($pH_{IEP}$ = 2.5 - 4.3) than is typically observed for anatase (e.g., $pH_{IEP}$ values of 5.2 - 6.0 were obtained for P25 and NAM),[27-28] which indicates that the titania frustules possess a stronger surface acidity than the commercial particles. The titania frustules also possessed significant differences in fluorine contents. The $TiOF_2$-based frustules contain a calculated 37.3% (by weight) of fluorine. This fluorine content dropped upon conversion of $TiOF_2$ into anatase and appeared to decrease as the second heat treatment temperature increases. In other words, the fluorine content dropped from 5.5% to 1.4% when the second heat treatment temperature was increased from 400 to 600°C (Table 2-1). Notably, the decline in residual F-content coincided with an increase in $pH_{IEP}$ (i.e., decreasing surface acidity) of the frustule replicas (Table 2-1).

### 2.3.2. Hydrolysis of organophosphorous esters in the presence of $TiO_2$

The hydrolysis reactions of MOX and MTH (structures available in Fig. 2-3) in the presence and absence $TiO_2$ particles without the involvement of light (i.e., non-

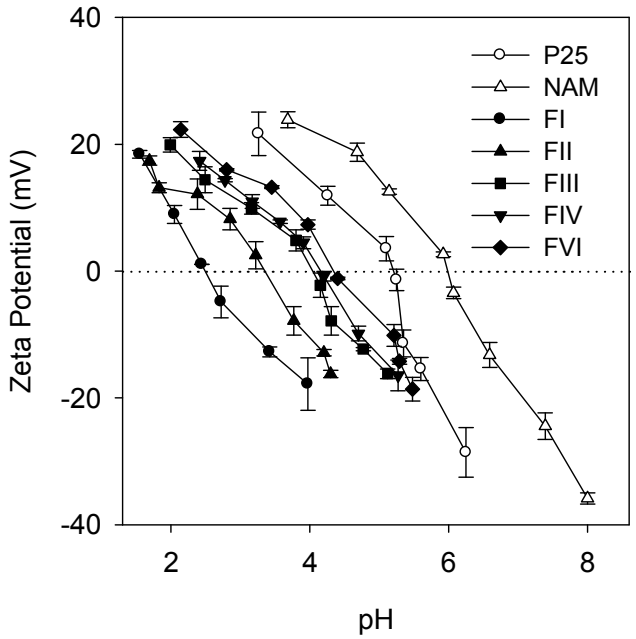


Figure 2-2. Zeta potentials of titania nanoparticles and titania-based frustule replicas in aqueous suspensions ($[TiO_2]$ = 0.1 g/L) as a function of pH.

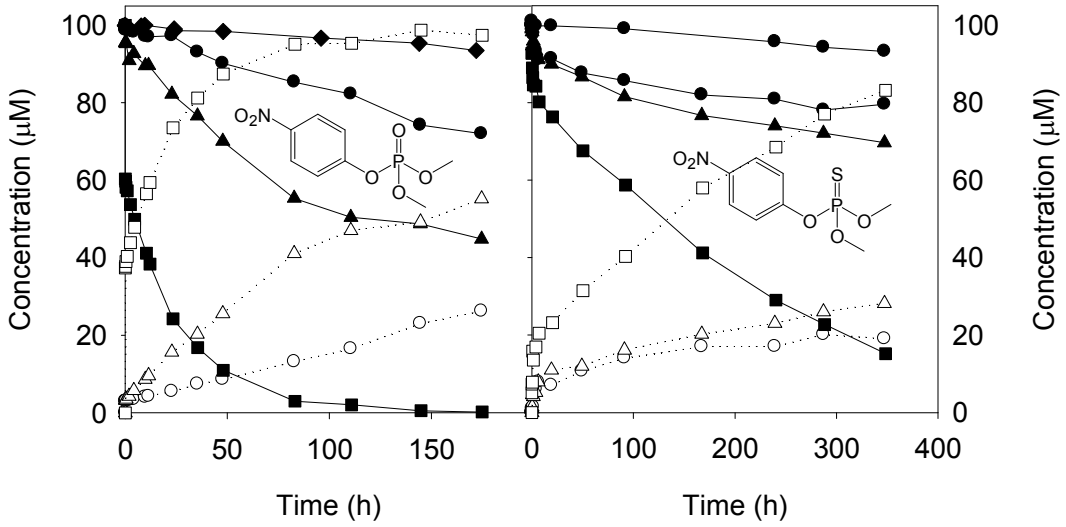


(a) (b)

Figure 2-3. Reaction time course of (a) MOX, and (b) MTH hydrolysis and 4-NP product generation in the presence and absence (control) of titania nanoparticles and titania-based frustule replicas: (♦) control; (●) P25 - parent compound; (○) P25 - 4-NP; (▲) NAM - parent compound; (Δ) NAM - 4-NP; (■) FII - parent compound; (□) FII - 4-NP (Reaction conditions: 1.0g/L $TiO_2$, 100 μM parent compound initially, 10 mM NaCl, 5 mM MOPS buffer (pH 6.3), 25°C).

photocatalytic) were studied. Experiments with $TiO_2$ particles conducted in amber borosilicate bottles, amber borosilicate bottles wrapped with aluminum foil, and clear borosilicate bottles under laboratory ambient light yielded nearly identical hydrolysis rate constants for MOX, confirming that light was not involved in the above reactions. All of the hydrolysis reactions followed pseudo-first-order kinetics fairly well. Least-square linear regressions of log parent compound concentration versus time plots yielded slopes corresponding to the pseudo-first-order rate constants ($k$) with $R^2$ values greater than 0.96. The pseudo-first-order rate constants obtained under different reaction conditions are summarized in Table 2-2. In all of the experiments, decay of MOX and MTH was matched by generation of the major product, 4-nitrophenol (4-NP), reaching >95% of overall mass balance throughout the reaction (Fig. 2-3). The observed good mass balance and the fact that the concentrations of MOX and MTH in the sample supernatants were very close to the added concentration (i.e., 100 μM) of the parent compound during the initial reaction period indicate that the adsorption of MOX, MTH and 4-NP to the $TiO_2$ particles (and to the reactor walls as well) is negligible.

As shown by Fig. 2-3 and Table 2-2, the hydrolysis of MOX was catalyzed by all of the $TiO_2$ particles examined; however, the catalytic effect was significantly stronger by the titania frustules than the commercial titania nanoparticles. For instance, the frustules ("FII" replica) increased the hydrolysis rate of MOX by as much as a factor of 130 relative to the control, whereas the NAM and P25 particles enhanced the rate by only factors of 15 and 6, respectively. This catalytic effect is quite dramatic when considering the oxides' specific surface areas. For example, although the FII titania replicas possessed a surface area of 4.2 $m^2/g$, 13 and 74 times lower than that for the P25 and NAM titania powder (i.e., 54.5 $m^2/g$ and 311.6 $m^2/g$, respectively), the hydrolysis rate of

Table 2-2. Pseudo-first-order rate constants ($k$) for the hydrolysis of MOX and MTH in the presence and absence of $TiO_2$ particles.

| | | Methyl Paraoxon 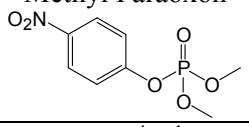 | | Methyl Parathion 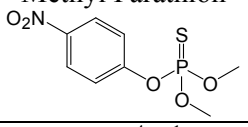 | |
|---|---|---|---|---|---|
| pH | $TiO_2$ particles | $k$ ($\times 10^{-4}$ $h^{-1}$) | $k/k_0$ [a] | $k$ ($\times 10^{-4}$ $h^{-1}$) | $k/k_0$ [a] |
| 4.5 | No oxide | 3.27 ± 0.53 | 1.0 | 1.57 ± 0.43 | 1.0 |
| | P25 | 13.43 ± 1.52 | 4.1 | 7.59 ± 2.67 | 4.8 |
| | NAM | 42.50 ± 1.48 | 13.0 | 7.88 ± 1.61 | 5.0 |
| | Frustule I (w/o oxd.) [b] | 222.9 ± 20.8 | 68.2 | 31.98 ± 1.37 | 20.4 |
| | Frustule II (400 °C) [c] | 334.9 ± 42.1 | 102.4 | 34.42 ± 3.60 | 21.9 |
| | Frustule III (450 °C) | | | | |
| | Frustule IV(480 °C) | | | | |
| | Frustule VI (600 °C) | 36.2 ± 1.36 | 11.07 | 6.21 ± 0.61 | 4.0 |
| 6.3 | No oxide | 3.62 ± 1.04 | 1.0 | 2.19 ± 0.50 | 1.0 |
| | P25 | 20.90 ± 1.10 | 5.8 | 7.23 ± 1.83 | 3.3 |
| | NAM | 54.86 ± 4.50 | 15.2 | 12.38 ± 1.49 | 5.7 |
| | Frustule I (w/o oxd.) | 373.0 ± 35.1 | 103.0 | 38.07 ± 1.62 | 17.4 |
| | Frustule II (400 °C) | 468.5 ± 101 | 129.4 | 40.31 ± 4.20 | 18.4 |
| | Frustule III (450 °C) | 248.4 ± 24.5 | 68.6 | | |
| | Frustule IV(480 °C) | 104.5 ± 6.18 | 28.9 | | |
| | Frustule VI (600 °C) | 68.54 ± 3.37 | 18.93 | 10.31 ± 1.19 | 4.7 |
| 7.9 | No oxide | 6.78 ± 0.72 | 1.0 | 2.98 ± 0.56 | 1.0 |
| | P25 | 25.90 ± 1.25 | 3.8 | 12.60 ± 1.72 | 4.2 |
| | NAM | 72.32 ± 3.57 | 10.7 | 13.66 ± 3.22 | 4.6 |
| | Frustule I (w/o oxd.) | 507.9 ± 49.5 | 74.9 | 47.91 ± 2.65 | 16.1 |
| | Frustule II (400 °C) | 799.3 ± 314 | 117.9 | 54.00 ± 6.56 | 18.1 |
| | Frustule III (450 °C) | | | | |
| | Frustule IV(480 °C) | | | | |
| | Frustule VI (600 °C) | 87.25 ± 4.86 | 12.9 | 11.56± 1.42 | 3.9 |

[a] $k_0$: the pseudo-first-order rate constant in the absence of $TiO_2$ catalyst; [b] without additional oxidation in preparation of $TiO_2$ frustule; [c] oxidation temperature in preparation of $TiO_2$ frustule (Reaction conditions: $[pesticide]_0$ = 100 μM, $[TiO_2]_0$ = 1.0 g/L, 5 mM pH buffer, 22°C).

MOX in the presence of the Frustule II titania was 22.4 and 8.5 times greater than those in the presence of the P25 and NAM titania, respectively (Table 2-2). For MTH, the catalytic effect by the various $TiO_2$ particles was in a similar trend but less pronounced. At the three pH values examined, the rate constants increased slightly with pH. The catalytic effects (i.e., $k/k_0$) were also quite similar, with only slight decrease as the pH was increased (Table 2-2). Interestingly, the titania frustules that were exposed to different temperatures during the reaction (2) treatment (fluorine removal) exhibited different catalytic reactivity; that is, titania frustules subjected to a higher temperature treatment exhibited a reduced catalytic effect.

The effect of titania dose was examined by using different dose of titania particles. As shown in Fig. 2-4, the higher the dose of each type of titania particles exhibited faster hydrolysis of MOX at pH 6.3, and there were good linearity between the titania dose and the pseudo-first-order rate constants ($k$) with $R^2$ values greater than 0.96. The relative catalytic activity of titania frustules to P25 and NAM, at the lower dose was very similar to that at 1.0 g/L $TiO_2$; at the concentration of $TiO_2$ of 0.5 g/L, the hydrolysis rate of MOX in the presence of FII was 27.4 and 9.5 times greater than those in the presence of P25 and NAM.

The comparison made earlier clearly indicate that the enhanced catalytic effect of titania frustules is not due to greater surface area. Surface morphology can also be ruled out to be a significant factor since no discernable morphological differences could be observed among the titania frustules that exhibited very different catalytic activity. Crystalline phase is unlikely the reason either since the titania frustules have essentially the same titania phase (i.e., anatase) as the NAM particles. Overall, the catalytic activity of titania frustules is most strongly correlated to the oxide's residual F-content, which is

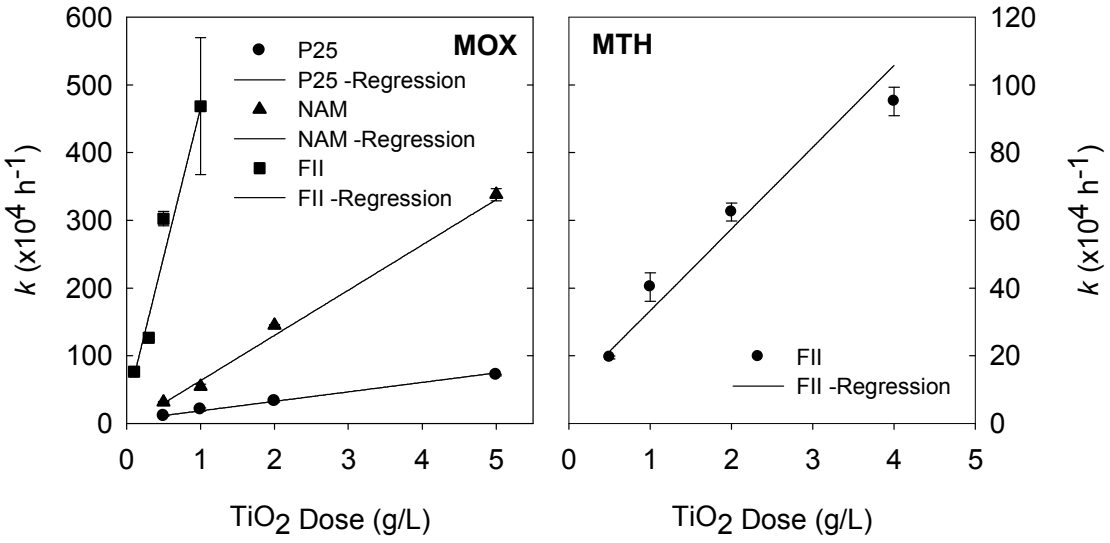


(a) (b)

Figure 2-4. Effect of the dose of $TiO_2$ on the hydrolysis of (a) MOX and (b) MTH (Reaction conditions: 100 μM MOX or MTH, 10 mM NaCl, 5 mM acetate buffer (pH 6.3), 25°C).

influenced by the temperature employed in the second heat treatment process, and to $pH_{IEP}$ (i.e., a measure of the surface acidity). The residual F-content and $pH_{IEP}$ are also strongly correlated with each other. As the residual F-content increases, the surface acidity increases (i.e., decreasing $pH_{IEP}$ value) and the titania frustules' catalytic activity also increases. This is consistent with the earlier studies that reported incorporation of fluorine in alumina and silica-alumina catalysts (F replacing surface or lattice O and OH groups) increases the acidity of both protonic (Bronsted) and nonprotonic (Lewis) sites on the surfaces because of the stronger electronegativity and polarizing effect of fluorine.[36-37] In analogy, the presence of fluorine in $TiO_2$ phase in this study results in increased Lewis acidity and excess positive charge on the surface-bound Ti(+IV), indicative by the lower $pH_{IEP}$ values of the titania frustules as the residual F-content increases.

It is well recognized that metal ions can catalyze hydrolysis of carboxylic esters, amides and phosphorous esters by (i) coordinating the compound in a manner that raises its susceptibility towards nucleophilic attack, (ii) coordinating the nucleophile in a manner that raises its reactivity toward electrophilic sites, or (iii) a combination of the above two mechanisms.[29-31] Mechanism (i) is strongly related to the ability of metal ions to coordinate the compound (e.g., the O atom of the P=O bond) and polarize electrons away from the nucleophilic site (e.g., the P center of the P=O bond). Mechanism (ii) is strongly tied to the ability of metal ions to induce the deprotonation of coordinated water through reactions such as:

$$Me^{2+} + H_2O = MeOH^{+} + H^{+}, \; *K1 = [MeOH^{+}][H^{+}]/[Me^{2+}].$$

Thus, metal ions of stronger Lewis acidity and greater affinity to the compound ligand donor atoms would be stronger catalysts. The catalysis of metal oxide surfaces on hydrolysis reactions is essentially similar to that of dissolved metal ions.[28,32-35]

Based on the above reasoning, the stronger surface acidity of titania frustules (resulted from F-doping) may lead to their stronger catalytic effect on the hydrolysis of MOX and MTH than the commercial P25 and NAM titania particles. The observation that MOX is much more susceptible than MTH to catalysis by the titania frustules may also be explained. MOX possesses a "hard" O donor atom that is likely to coordinate more strongly to the "hard" Ti(+IV) metal center than MTH's "soft" S donor atom,[38] thus rendering a stronger catalysis via Mechanism (i). Sulfur is also less electronegative than oxygen, resulting in less electrophilic and consequently less reactive phosphorous center in the thionates than in the oxonates.

### 2.3.3. Hydrolysis of carboxylic esters in the presence of $TiO_2$

The catalytic effect of titania particles were also examined for the hydrolysis of three carboxylic esters, MS, MB and MAMB (structures available in Fig. 2-5), at pH 7.0. As shown in Fig. 2-5, measurable hydrolysis of MS and MB occurred in the absence of titania particles with pseudo-first-order rate constants $4.12 \times 10^{-3}$ $h^{-1}$ and $8.04 \times 10^{-3}$ $h^{-1}$, respectively. MAMB, on the other hand, was quite stable within 150 hours of reaction time ($k < 1.0 \times 10^{-4}$ $h^{-1}$). When titania particles were added, all of the hydrolysis reactions were catalyzed by the $TiO_2$ particles used in this study. In this case, P25 exerted the strongest catalytic effect on the hydrolysis of these three carboxylic esters. The catalytic activities of titania frustules and NAM were comparable, both lower than

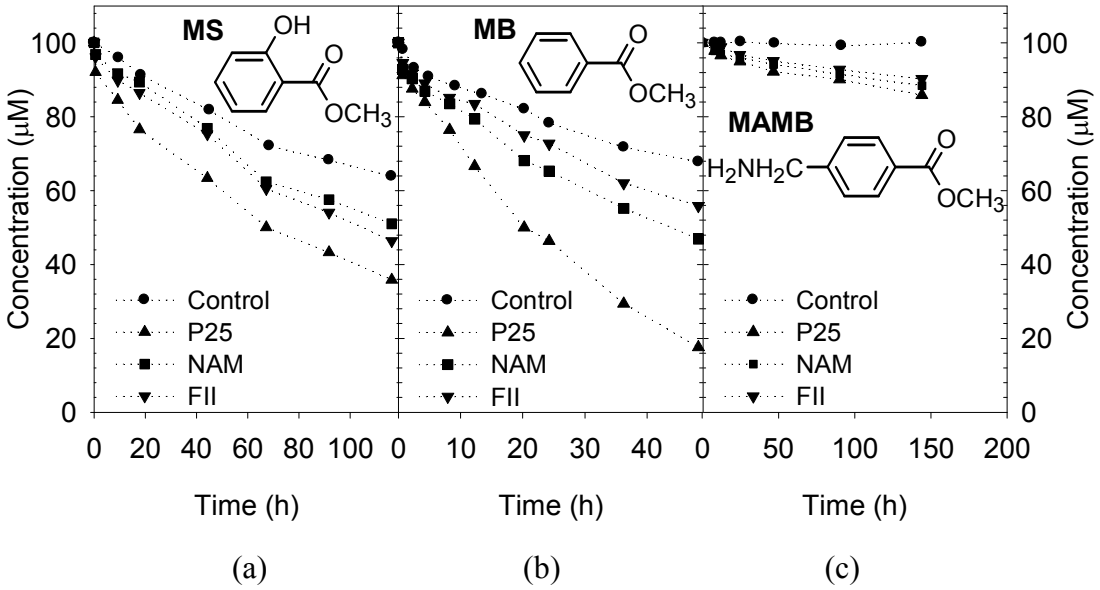


Figure 2-5. Hydrolysis of MS, MB and MAMB in the absence (control) and presence of $TiO_2$ (Reaction conditions: 1.0g/L $TiO_2$, 100 μM parent compound initially, 10 mM NaCl, 5 mM acetate buffer (pH 7.0), 25°C).

that of P25. For MS, the rate constant with FII was $6.51 \times 10^{-3}$ $h^{-1}$, slightly higher than that with NAM ($5.91 \times 10^{-3}$ $h^{-1}$), whereas for MB and MAMB, the rates with FII were 76% and 90% of those with NAM, respectively. MAMB hydrolyzed most slowly and the difference among the catalytic activities of the three $TiO_2$ particles was quite small. The data also indicate that the adsorption of these three carboxylic esters to the $TiO_2$ oxide surfaces is negligible (Fig. 2-5).

Despite that the adsorption of the selected esters to $TiO_2$ particles did not appear to be significant, the adsorption capacities of the three groups of titania particles were examined separately. This is based on the consideration that adsorption of chemical agents to the catalyst surface is a critical step for surface-catalyzed hydrolysis (i.e., via the Mechanism (i)).[28,34] Fluorine doping of $TiO_2$ may potentially affect the surface adsorption capacity. Two carboxylic acids, SA and BA (also the hydrolysis products of MS and MB, respectively), were selected for these experiments. 10 μM of SA or BA was allowed to equilibrate with 1 g/L of $TiO_2$ particles for three days at pH 4 and 7 for SA and at pH 3 and 7 for BA. After three days, sample aliquots were centrifuged. The amount adsorbed was determined based on the difference in the original concentration and the concentration in the supernatants. Control experiment in the absence of titania particles showed that the adsorption of SA and BA to the reactor walls was 1.3 - 5.9% and did not have significant influence on the adsorption to titania particles.

The amounts of SA and BA adsorbed per mass of titania were greatest for NAM, and the lowest for titania frustules (FII as the example) (Fig. 2-6(a) and (b)); this is consistent with the surface areas among the three oxides, where the surface area is highest for NAM and lowest for titania frustules. However, if normalized by specific surface area, the amount of SA and BA adsorbed per unit area was greatest for FII,

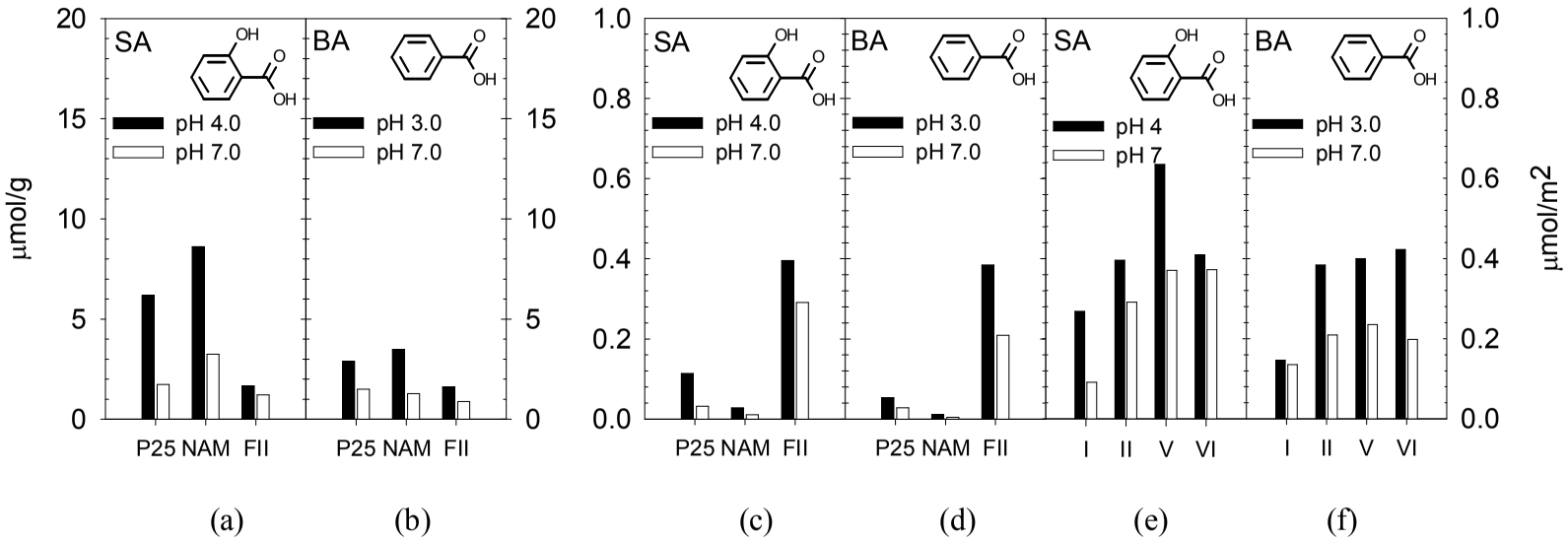


Figure 2-6. Adsorption of SA and BA to the titania particles: (i) the amount of adsorbed (a) SA, (b) MA per unit mass of $TiO_2$; (ii) the amount of adsorbed (c) SA and (d) BA per specific surface area of $TiO_2$; (iii) the amount of adsorbed (e) SA and (f) BA per specific surface area of $TiO_2$ frustules (FI-VI).

followed by P25 and then NAM (Fig. 2-6(c) and (d)). Among the different frustule replicas, the difference in the amounts of acids adsorbed was not significant. Most notably, the adsorption of both acids to FI was lower than to the other frustule replicas (i.e., FII, V and VI) (Fig. 2-6(e) and (f)). The difference in the adsorption capacity on the per unit area basis could be partly resulted from the difference in crystalline structures and surface properties of $TiO_2$ particles. P25 is a mixture of two titania phases while NAM is pure anatase. FI contains the $TiOF_2$ phase while the other frustule replicas are predominantly anatase crystals based on the XRD and TEM analysis.

Also as shown in Fig. 2-6, the adsorption of SA is generally stronger than BA. This can be explained by the fact that SA possesses an auxiliary hydroxyl functional group in addition to the carboxylate group to facilitate complexation with surface-bound Ti(IV) ions and thus enhances the adsorption. In all cases, adsorption was greater at the acidic pH (3-4) than at the neutral pH (7). This tend is consistent with the charge effects expected from the $pK_a$ of the acids and the $pH_{IEP}$ of the surfaces. The $pK_a$'s of SA and BA are 2.97 and 4.20, respectively.[56] The $pH_{IEP}$ values of P25, NAM and FII are 5.2, 6.0, and 3.3 respectively (Table 2-1). At pH 7, electrostatic repulsion between the negatively charged deprotonated acids and the negatively charged oxide surfaces led to lower adsorption. At pH 3-4, the surfaces of P25 and NAM were positively due to their higher $pH_{IEP}$ while the surface of titania frustules FII was still negatively charged. The positively charged surfaces would be more susceptible to adsorption by negatively or neutral charged SA and BA molecules than negatively charged surfaces.

Overall, the adsorption experiments show that the specific surface area is most critical in determining the net adsorption capacity of a given mass of titania oxide.

However, when normalized by the specific surface area, the F-doped titania frustules have higher adsorption capacity on per unit area basis than the non-F-doped P25 and NAM implies that F-doping might enhance adsorption. However, such adsorption capacity did not follow the trend of residual F-content among various F-doped anatase frustule replicas (i.e., FII, V and VI). Further studies are needed to discern the effect of F-doping of titania on the adsorption to its surfaces.

### 2.3.4. F- leaching from $TiO_2$ frustules

Because the catalytic activity of titania frustules appeared to be strongly related to the F-content of the frustules, the possibility of dissolution of fluorine from the titania frustules into the reaction solution was investigated. It was found that the F-doped titania frustules leached fluorine to form fluoride ions in aqueous solutions. As shown by Fig. 2-7, the titania frustules lost fluorine rather quickly to yield high concentrations of fluoride ions in the reaction solution. For instance, the leaching of fluorine from FII was rapid enough that within the first hour of the hydrolysis reaction, the concentration of fluoride increased to above 1 mM and gradually reached to a plateau at around 1.5 mM. These experiments were conducted at 1.0 g/L of titania frustules in 20 mL of reaction volume. Based on the fact that the residual fluorine in frustule II is 5.5% by weight, the maximum amount of fluorine that can be leached from FII is 1.1 mg. Therefore, 1.5 mM of fluoride ion concentration, which is equivalent to 0.57 mg of fluorine accounts for 52% of leaching. Although by different extent, all three titania frustules examined were found to leach fluoride (Fig. 2-7). Significantly, the extent of fluorine leaching from the

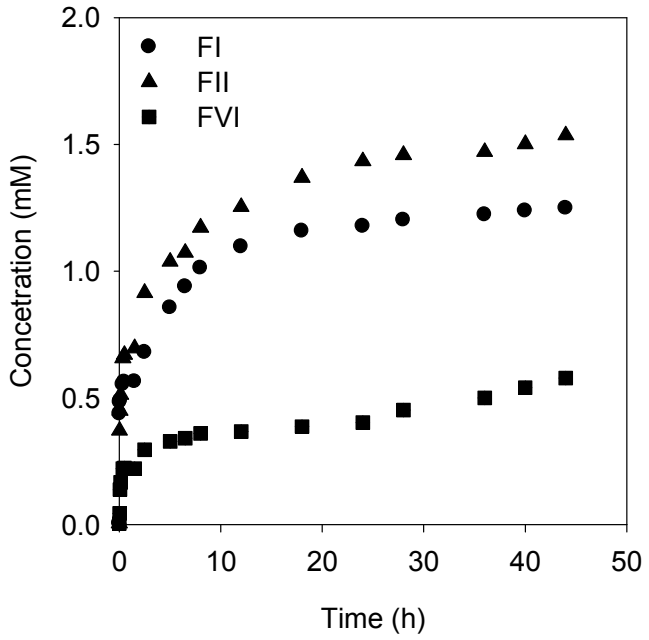


Figure 2-7. Time course of fluorine leaching from titania frustule replicas (Reaction conditions: 1.0g/L $TiO_2$, 5 mM MOPS buffer (pH 7.0), 25°C).

frustules I, II and VI was in agreement with their catalytic hydrolysis rate constants of MOX, i.e., the faster hydrolysis rate constants, the higher fluoride ion concentration leached from the frustules in the order of FII>FI>FVI (Fig. 2-7 and Table 2-2).

After the fluorine leaching experiment, the reaction solution was filtered and the captured frustule II particles were dried and then used again in a separate kinetic experiment of MOX hydrolysis to evaluate their catalytic effect. The reused frustule II yielded a rate constant of $42.9 \times 10^{-4}$ $h^{-1}$ at pH 7 for the hydrolysis of MOX. Compared to the rate constants obtained in the original tests (i.e., $468.5 \times 10^{-4}$ $h^{-1}$ at pH 6.3, and $507.9 \times 10^{-4}$ $h^{-1}$ at pH 7.9 (Table 2), the loss of fluorine from the titania frustules resulted in significant decrease in the catalytic activity. Based on this observation, the leached fluoride ions in the solution likely play a critical role in the faster hydrolysis of MOX and MTH.

### 2.3.5. Effect of fluoride on hydrolysis

Knowing that fluoride ions were present in the reaction suspensions with titania frustules due to fluorine leaching of these materials, the effect of fluoride ions alone on the hydrolysis reactions was investigated by adding NaF to reaction solutions containing MOX or MTH but without any titania oxides. The added fluoride ion concentration ranged from 0.1 μM to 1000 μM. As shown in Fig. 2-8(a), the rate of MOX hydrolysis was greater with higher concentration of fluoride ions added. At above 10 μM of fluoride ion concentration, the rate constants of MOX and MTH increased proportionally

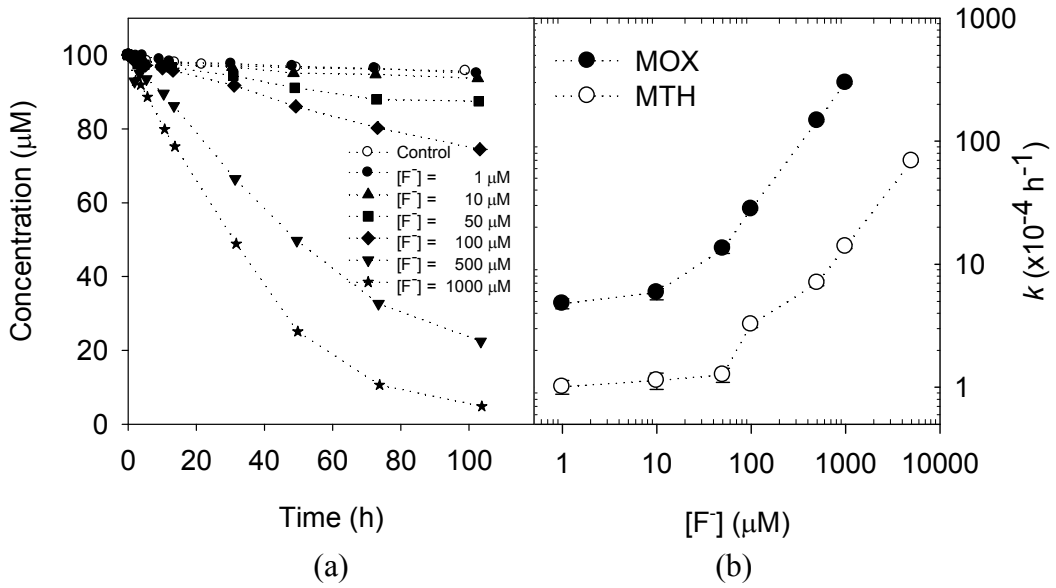


(a) (b)

Figure 2-8. (a) Hydrolysis of MOX in the presence of fluoride ions and comparison with the hydrolysis in the presence of titania frustule replicas (FII), and (b) hydrolysis rate constants for MOX and MTH as a function of dissolved fluoride ions.

with increasing fluoride ion concentration (100 μM of MOX and MTH initially) (Fig. 2-8(b)).

Fig. 2-9 shows the results of adding NaF with P25 or NAM to the hydrolysis of MOX at pH 7.0. Evidently, as the concentration of added fluoride ions increased, faster hydrolysis of MOX was observed. The hydrolysis rates of MOX were quite similar whether P25 or NAM was involved in the system, indicating the dominating role of fluoride ions in these reactions.

Experiments were also conducted to evaluate the effect of fluoride ions on the hydrolysis of carboxylic esters MS, MB, and MAMB. In contrast to the observations with MOX and MTH, adding NaF at the range of 0.1 to 1.5 mM did not result in any enhancement in the hydrolysis of MS, MB, and MAMB in the absence of titania particles.

The observations with MOX and MTH are consistent with the previous studies that showed fluoride ions as nucleophilic catalysts for the hydrolysis of organophosphorous esters. In the previous study by Mentz and Modro,[57] the catalytic effect of fluoride ions on the hydrolysis of aryl phosphates was demonstrated. In this study, fluoride ion had no effect on the demethylation of trimethyl phosphate, but had a profound effect on the hydrolysis of mixed aryl phosphate esters. Several alkali metal and tetramethylammonium fluoride salt, with LiF as an exception, all exhibited significant catalytic effect. For example, the hydrolysis of MOX was accelerated by $M^+F^-$ ($M^+ = K^+$, $Cs^+$, $Me_4N^+$) by a factor of ca. $8 \times 10^3$. Ogilvie *et al*. also reported that fluoride ions are catalysts in the transesterification reactions.[58] In their study, when a bis(trichloroethyl) alkyl phosphate was dissolved in isopropyl alcohol with CsF, trichloroethyl groups were replaced by isopropyl groups sequentially. These reactions

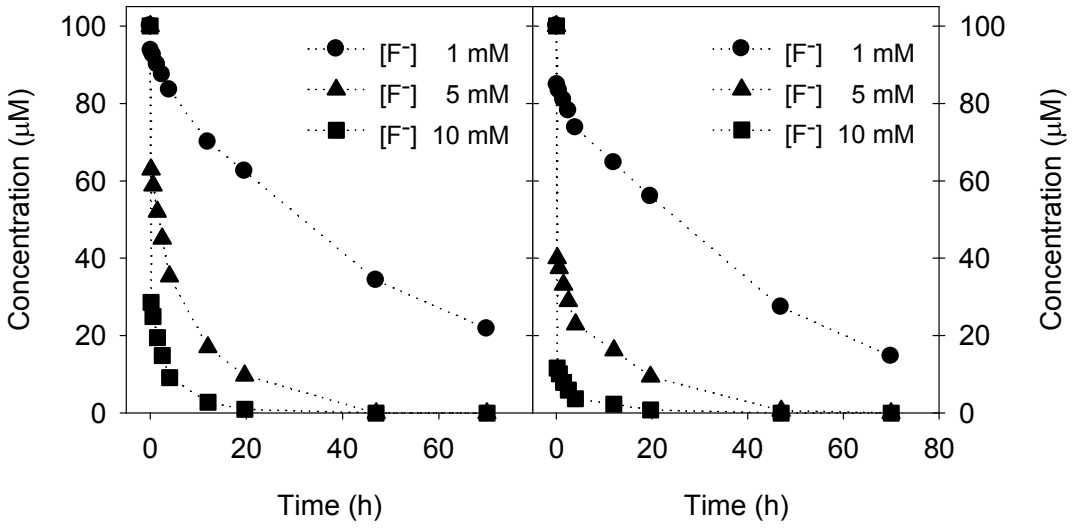


Figure 2-9. Effect of the addition of fluoride ions in the presence of $TiO_2$ particles, (a) P25 and (b) NAM.

occurred equally in the presence of tetra-*n*-butylammonium fluoride in place of cesium fluoride but not in the absence of fluoride ions. In addition, electronic structure calculations by Vincent and Hillier on a number of model systems using Gaussian proved that the solvated fluoride ion can act as a good nucleophile.[59]

Aside from the experimental results presented earlier in this section, the effect of pH on the hydrolysis of MOX in the presence of titania frustule II is also consistent with the suggestion that fluoride ions are nucleophilic catalysts. In this case, dissolved fluoride ions (leached from the frustules) are present in the solution and their speciation is affected by solution pH. The $pK_a$ of hydrofluoric acid is about 3.2, and thus protonation of $F^-$ occurs at below pH 3.2 to yield the HF species, which is a much weaker nucleophile than $F^-$ (Fig. 2-10(a)). As shown in Fig. 2-10(b), the hydrolysis rate of MOX was considerably slower at pH 2.5 and increased with increasing pH. This significant slowdown of hydrolysis rate agrees with the conversion of $F^-$ to the less effective HF nucleophile. Overall, the observations in this study are consistent with the previous reports that indicate fluoride ions can catalyzed the hydrolysis of organophosphorous esters.

For carboxylic esters, 2-pyridyl acetate was tested for the hydrolysis in the presence of various fluoride salts and no nucleophilic hydrolysis was observed in the previous study by Mentz and Modro.[57] Even though the catalytic activity of fluoride ions on the hydrolysis of carboxylic acid anhydrides has been reported,[60] no other studies have reported significant catalytic activity of fluoride ions on the hydrolysis of carboxylic acid esters or other hydrolyzable compounds. The negligible catalysis by fluoride ions and the lack of enhanced catalytic effect by the titania frustules on the hydrolysis of carboxylic

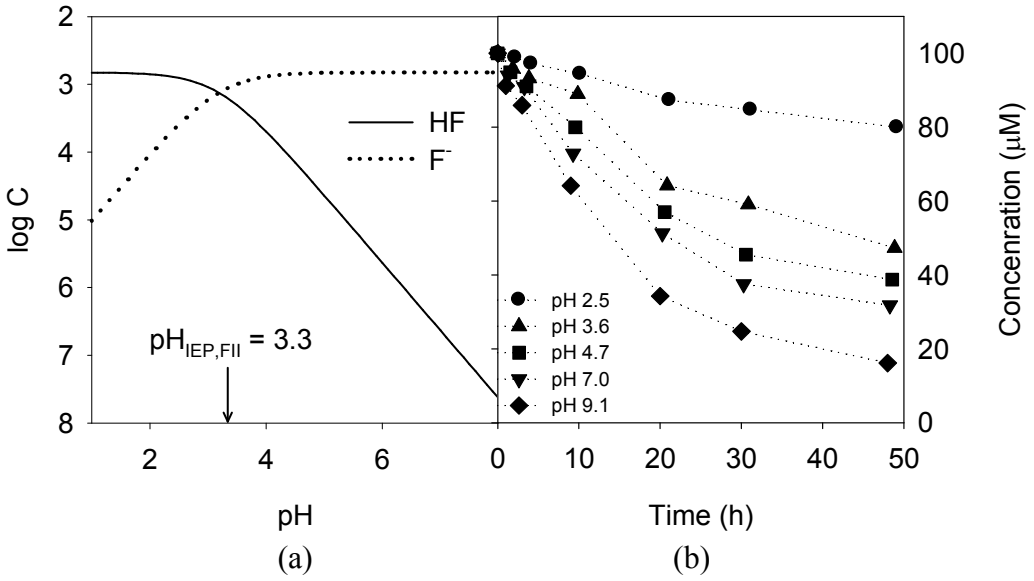


Figure 2-10. Effect of pH on the fluoride ion catalyzed hydrolysis: (a) pC-pH diagram of hydrofluoric acid with the total concentration of fluoride at 1.5 mM, and (b) pH effect on the hydrolysis of MOX.

esters strongly support that the enhanced hydrolysis of MOX and MTH is mostly due to the leached fluoride ions from the titania frustules.

### 2.3.6. Product distribution comparison

Depending on the reaction conditions and the alcohol moieties present in organophosphorous esters, different hydrolysis mechanisms may predominate.[43] As shown in Scheme 1, the hydrolysis of MOX and MTH may yield the P-O and C-O cleavage products. In the former pathway, nucleophiles can attack the electron-deficient phosphorus center of MOX and MTH, causing the P-O bond to cleave and yield the final products of 4-NP and dimethyl(thio)phosphate. In the latter pathway, the carbon attached to the phosphate oxygen is attacked by a nucleophile and the C-O bond is cleaved to yield methyl 4-nitrophenyl (thio)phosphate and methanol products. The relative distribution between these two reaction pathways was further investigated to assess the involvement of fluoride ions in the studied systems.

Overall, in all of the reactions 4-NP was monitored and found to be a dominant product (typically accounted for >95% of the products) and only small amounts of methyl 4-nitrophenyl phosphate or thiophosphate were generated. In the homogeneous hydrolysis reactions of MOX catalyzed by different concentration of fluoride ions, different amounts of the C-O cleavage product (i.e., methyl 4-nitrophenyl phosphate) were generated after the same degradative conversion of the parent compound (Fig. 2-11(a)). Although the amount of the C-O cleavage product was small, the difference among these reactions was clearly seen; that is, the lesser amount of the C-O cleavage

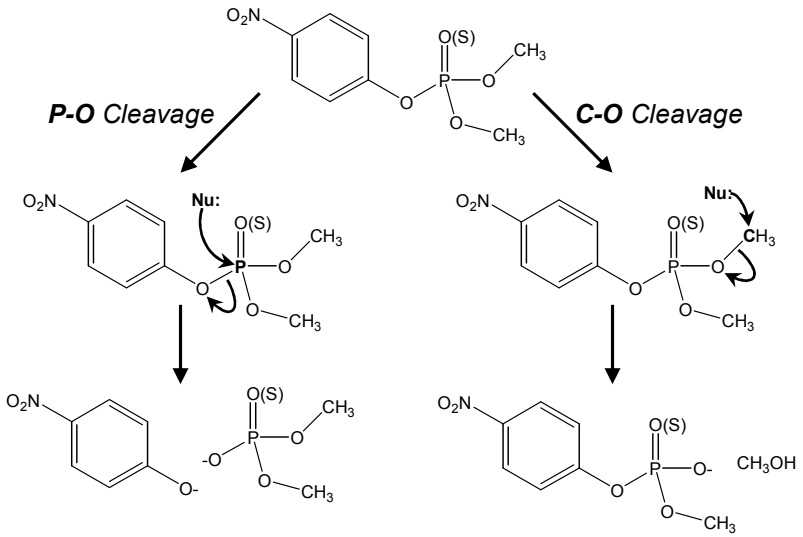


Scheme 1. Pathways of organophosphorous ester hydrolysis.

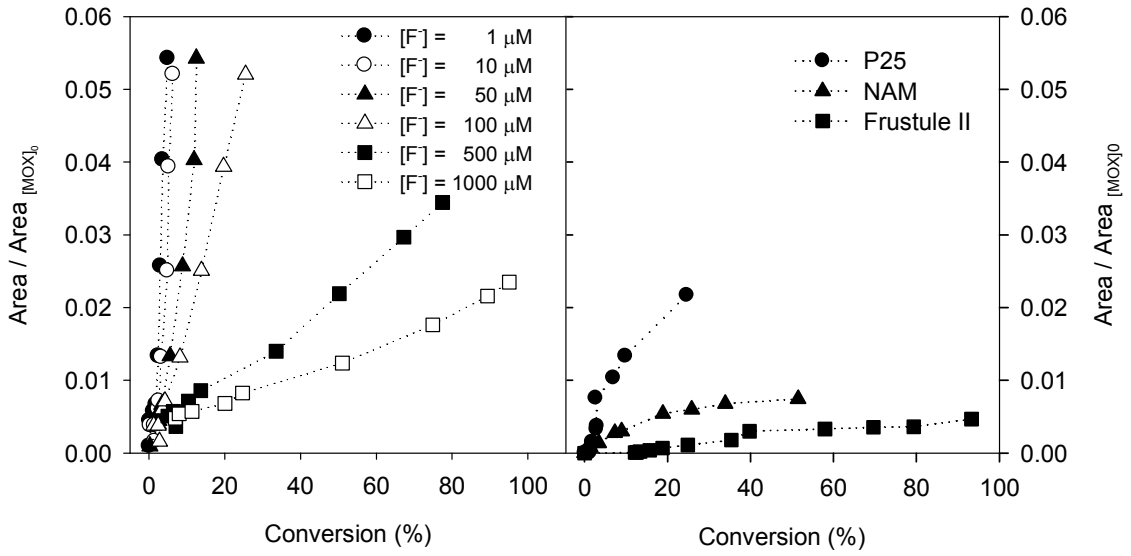


(a) (b)

Figure 2-11. Evolution of C-O cleavage products as a function of conversion of MOX under (a) homogenous condition in the presence of fluoride ions, and (b) heterogeneous condition in the presence of titania particles.

product was detected at the higher concentration of added fluoride ions. In Fig. 2-11, the areas of the C-O cleavage product peak in the HPLC spectra were used for quantitative comparison due to the lack of authentic standards for this product, methyl 4-nitrophenyl phosphate. However, the product identity of methyl 4-nitrophenyl phosphate was confirmed by LC/MS analyses.

Different types of $TiO_2$ particles also affected the distribution of the hydrolysis products (Fig. 2-11(b)). Greater amounts of the C-O cleavage product were generated in the presence of P25 and NAM (without fluoride ions), whereas lesser amounts of the C-O cleavage product was detected in the presence of titania frustules (FII), which contained residual fluorine and released fluoride ions into the reaction solution.

As a nucleophile, fluoride ions can compete with other nucleophiles such as $OH^-$ for the hydrolysis and may affect the distribution of hydrolysis products. In the hydrolysis reactions of mixed esters, nucleophilic displacement reaction can take place both at the phosphorous atom with an alcohol moiety being the leaving group, and at the carbon bound to the oxygen of an alcohol moiety with the diester being the leaving group. In general, the most basic group is subject to this displacement. Base-catalyzed reaction generally occurs at the phosphorous atom leading to the dissociation of the alcohol moiety that is the best leaving group (P-O cleavage) by the reaction as shown in the previous study for an analog compound, parathion which has ethyl alcohol moieties instead of methyl groups in MTH.[61] Depending on the nature of the leaving groups, the neutral reaction may also proceed by nucleophilic substitution at the carbon atom.

As shown in the study by Mentz and Modro,[57] dimethyl phosphate was the only product of the hydrolysis of MOX in the presence of one mole equivalent of metal

fluoride salt in $D_2O$-[$^2H_6$] acetone (1:1 v/v) at 60$^o$C, while the ratios of the rates for the reaction at the methyl carbon ($k_c$) and the reaction at the phosphorus atom ($k_p$), $k_c/k_p$ was 2.2 in the absence of $M^+F^-$ salt ($M^+$ = $Na^+$, $K^+$, $Cs^+$, $Me_4N^+$).[57,62] These results demonstrate that fluoride ions exert regioselectivity for nucleophilic attack at the phosphorous center.

Even though the specific reaction conditions are not identical between this investigation and the earlier studies, lower generation of the C-O cleavage product was observed in the presence of sodium fluoride salt. While a penta-coordinated fluorinated phosphate intermediates was postulated and detected in the previous study,[63] such intermediates could not be confirmed in the LC/MS spectra.

## 2.4. Conclusions

The amount of residual fluorine in the anatase frustules can be controlled by materials preparation conditions. This F-doping leads to lower $pH_{IEP}$ and stronger acidity for the surfaces. These two parameters could potentially promote the catalytic activity of oxide surfaces to facilitate hydrolysis of organic compounds. However, in this study significant fluorine leaching from the 3-D titania frustules occurred. The leached fluoride ions in the solution appear to be the dominating factor that contributes to the much faster hydrolysis rate of organophosphorous esters MOX and MTH. The analysis of hydrolysis products support the above conclusion and also suggest that fluoride ions are nucleophilic catalysts in these reactions. Because the hydrolysis of carboxylic esters are not susceptible to catalysis by fluoride, significantly enhanced hydrolysis rates of these compounds were not observed in the presence of titania frustules affecting the observed catalytic effect and can be leached from frustules as $F^-$ in aqueous systems. Although the titania frustules do possess stronger surface acidity that favors catalysis in hydrolysis reactions, this effect is likely difficult to be seen given the low surface areas of these materials and in the presence of the strong effect of fluoride ions due to its high concentration.

**Acknowledgement**

This material is based upon work partially supported by the National Science Foundation (Dr. Patrick Brezonik, Program Manager) and Air Force Office of Scientific Research (Dr. Joan Fuller, Dr. Hugh DeLong, Program Managers).

# REFERENCES


1. C. L. Carnes and K. J. Klabunde, *J. Mol. Catal. A.*, 2003, **194**, 227.

2. P. Li, D. E. Miser, S. Rabiei, R. T. Yadav and M. R. Hajaligol, *Appl. Catal. B*, 2003, **43**, 151.

3. J. C. Yu, J. Yu, L. Zhang and W. Ho, *J. Photochem. Photobiol. A*, 2002, **148**, 263.

4. H. Kominami, H. Kumamoto, Y. Kera and B. Ohtani, *J. Photochem. Photobiol. A*, 2003, **160**, 99.

5. A. I. Kontos, I. M. Arabatzis, D. S. Tsoukleris, A. G. Kontos, M. C. Bernard, D. E. Petrakis and P. Falaras, *Catal. Today*, 2005, **101** [3-4], 275.

6. L. Gao, *Mater. Integration*, 2004, **17**, 43.

7. N. Burniston, C. Bygott and J. Stratton, *Surf. Coat. Int. Part A*, 2004, **87**, 179.

8. M. Tomkiewicz and S. Kelley, in *Nanoparticles and Nanostructured Films*, ed. J. H. Fendler, Wiley-VCH Verlag GmbH, Weinheim, 1998, pp. 263-274.

9. N. Serpone and R. F. Khairutdinov, in *Semiconductor Nanoclusters: Physical, Chemical, and Catalytic Aspects*, Studies in Surface Science and Catalysis, vol. 103, Elsevier, Amsterdam, 1997, pp. 417-444.

10. M. R. Hoffmann, S. T. Martin, W. Choi and D. W. Bahnemann, *Chem. Rev.*, 1995, **95**, 69.

11. M. A. Fox and M. T. Dulay, *Chem. Rev.*, 1993, **93**, 341.

12. M. B. Green, G. S. Hartley and T. F. West, *Chemicals for Crop Improvement and Pest Management*, 3rd edition, Pergamon Press, Oxford, England, 1987.

13. E. Bauerlein, *Angew. Chem. Int. Ed.*, 2003, **42**, 614..

14. M. Hildebrand and R. Wetherbee, in *Progress in Molecular and Subcellular Biology*, ed. W. E. G. Muller, vol. 33, Springer-Verlag, Berlin, 2003, pp. 11-57.

15. S. A. Crawford, M. J. Higgins, P. Mulvaney and R. Wetherbee, *J. Phycol.*, 2001, **37**, 542.

16. D. G. Mann and S. J. M Droop, *Hydrobiologia*, 1996, **336**, 19.

17. F. E. Round, R. M. Crawford and D. G. Mann, *The Diatoms: Biology and Morphology of the Genera*, Cambridge Univ. Press, New York, 1990.

18. E. L. Duke and B. E. F. Reimann, in *The Biology of the Diatoms*, ed. D. Werner, Univ. California Press, Berkeley, CA, 1977, pp. 65-109.

19. T. Lebeau and J.-M. Robert, *Appl. Microbiol. Biotechnol.*, 2003, **60**, 612.

20. V. Martin-Jezequel, M. Hildebrand and M. A. Brezinski, *J. Phycol.*, 2000, **36**, 821.

21. E. O. Duerr, A. Molnar and V. Sato, *J. Mar. Biotechnol.*, 1998, **7**, 65.

22. R. R. Unocic, F. M. Zalar, P. M. Sarosi, Y. Cai and K. H. Sandhage, *Chem. Commun.*, 2004, **7**, 796.

23. K. H. Sandhage, R. L. Snyder, G. Ahmad, S. M. Allan, Y. Cai, M. B. Dickerson, C. S. Gaddis, M. S. Haluska, S. Shian, M. R. Weatherspoon, R. A. Rapp, R. R. Unocic, F. M. Zalar, Y. Zhang, M. Hildebrand, B. P. Palenik, *Int. J. Appl. Ceram. Technol.*, 2005, **2**, 317.

24. K. H. Sandhage, *US Pat Appl.*, 20030099763, 2003.

25. T. Ohno, K. S. Sarukawa, K. Tokieda, M. Matsumura, *J. Catal.*, 2001, **203**, 82.

26. *Annual Book of ASTM Standards*, Vol. 12.01, ASTM International, West Conshohocken, PA, 2002, C 1502-01.

27. D. P. Minh, P. Gallezot and M. Besson, *Appl. Catal. B*, 2006, **63**, 68.

28. A. Torrents and A. T. Stone, *Environ. Sci. Technol.*, 1991, **25**, 143.

29. C.-H. Huang and A. T. Stone, *Environ. Sci. Technol*., 2000, **34**, 4117.

30. J. M. Smolen and A. T. Stone, *Environ. Sci. Technol.*, 1997, **31**, 1664.

31. J. Chin, *Acc. Chem. Res.*, 1991, **24**, 145.

32. J. M. Herrmann, C. Guillard, M. Arguello, A. Aguera, A. Tejedor, L. Piedra and A. Fernandez-Alba, *Catal. Today*, 1999, **54**, 353.

33. J. M. Smolen and A. T. Stone, *Soil Sci. Soc. Am. J.*, 1998, **62**, 636.

34. C.-H. Huang and A. T. Stone, *J. Agric. Food Chem.*, 1999, **47**, 4425.

35. A. Torrents and A. T. Stone, *Soil Sci. Soc. Am. J.*, 1994, **58**, 738.

36. G. Seo, N.-H. Kim, Y.-H. Lee and J.-H. Kim, *Catal. Lett.*, 1998, **51**, 101.

37. A. K. Ghosh and R. A. Kydd, *Catal. Rev. Sci. Eng.*, 1985, **27**, 539.

38. J. E. Huheey, E. A. Keiter and R. L. Keiter, *Inorganic Chemistry*, 4th edition, Hapers Collins College Publishers, New York, 1993.

39. G. P. Fulton, *Diatomaceous Earth Filtration for Safe Drinking Water*. American Society of Civil Engineers, Reston, VA, 2000.

40. D. Li, H. Haneda, N. K. Labhsetwar, S. Hishita and N. Ohashi, *Chem. Phys. Lett.*, 2005, **401**, 579.

41. H. Park, and W. Choi, *J. Phys. Chem. B.*, 2004, **108**, 4086.

42. J. C. Yu, J. Yu, W. Ho, Z. Jiang and L. Zhang, *Chem. Mater.*, 2002, **14**, 3808.

43. R. P. Schwarzenbach, P. M. Gschwend, and D. M. Imboden, *Environemtnal Organic Chemistry*, 2nd edition, John Wiley & Sons, New York (2002), pp. 13-16, 538-540.

44. R. Asahi, T. Morikawa, T. Ohwaki, K. Aoki, Y. Taga, *Science* 2001, **293**, 269.

45. B. Kosowska, S. Mozia, A.W. Morawski, B. Grzmil, M. Janus, K. Kałucki, *Solar Energy Mater. Solar Cells* 2005, **88**, 269.

46. M. Janus, M. Inagaki, B. Tryba, M. Toyoda and A.W. Morawski, *Appl. Catal*. B., 2006, **63**, 272.

47. L. Li, W. Zhu, P. Zhang, Z. Chen and W. Han, *Wat. Res*., 2003, **37**, 3646.

48. D. Hufschmidt, D. Bahnemanna, J. J. Testa, C. A. Emilio and M. I. Litter, *J. Photoche. Photobiol*. A., 2002, **148**, 223.

49. H. Yamashit, M. Harada, J. Misaka, M. Takeuchi, K. Ikeue and M. Anpo, *J. Photochem. Photobiol*. A., 2002, **148**, 257.

50. M. S. Vohra and K. Tanaka, *Wat. Res*., 2003, **37**, 3992.

51. M. C. Hidalgo, G. Colon and J. A. Navıo, *J. Photochem. Photobiol*. A., 2002, **148**, 341.

52. B. Adamczyk, O. Boese, N. Weiher, S. L. M. Schroeder, and E. Kemnitz, J. *Fluorine Chem*., 2000, **101**, 239.

53. C. Minero, G. Mariella, V. Maurion and E. Pelizzetti. Lamuire, 2000, **16**, 2632-2641.

54. J. A. Cowan, *Inorganic Biochemistry: An Introduction*, VCH Publishers, Inc., New York (1993).

55. S.-J. Lee, S. Shaian, C.-H. Huang and K. H. Sandhage, *Chem. Commun*., 2006, Submitted.56. D. C. Harris, *Qunatitative Chemical Analysis*, 3rd edition, W. H. Freeman and Company, New York, 1991, p. 186, 261.

57. M. Mentz and T. A. Modro. *J. Chem. Soc., Perkin Tras*., 1995, **2**, 2223.

58. K. K. Ogilvie, S. L. Beaucage, N Theriault and D. W. Enwistle, *J. Am. Chem. Soc*., 1977, **99**, 1277.

59. M. A. Vincent and I. H. Hillier, *Chem. Commun*., 2005, **47**, 5902.

60. C. A. Bunton and J. H. Fendler, *J. Org. Chem*., 1967, **32**, 1547.

61. P. W. C. Barnard, C. A. Bunton, D. R. Llewellyn, C. A. Vernon and V. A. Welch, *J. Chem. Soc.* Part III, 1961, 2670.

62. M. Mentz, A. M. Modro and T. A. Modro, *J. Chem. Soc., Chem. Commun*, 1994, 1537.

63. R. J. P. Corriu, J.-P. Dutheil and G. F. Laneau, *J. Chem. Soc., Chem. Commun*, 1981, 101.